#### **CANCER IMMUNOLOGY**

# Multimodal delineation of a layer of effector function among exhausted CD8 T cells in tumors

Arja Ray<sup>1,2</sup>†, Molly Bassette<sup>1,2</sup>, Kenneth H. Hu<sup>1,2</sup>‡, Lomax F. Pass<sup>1,2</sup>, Tristan Courau<sup>1,2</sup>, Bushra Samad<sup>2,3</sup>, Alexis J. Combes<sup>1,2,3,4</sup>, Vrinda Johri<sup>2,3</sup>, Brittany Davidson<sup>2,3</sup>, Katherine Wai<sup>5</sup>, Patrick Ha<sup>5</sup>, Grace Hernandez<sup>6</sup>, Itzia Zaleta-Linares<sup>1,2</sup>, Matthew F. Krummel<sup>1,2</sup>\*

Undescribed functional axes may intersect with the trajectory of T cell exhaustion ( $T_{EX}$ ) to contribute to the antitumoral functions of CD8 T cells. By leveraging fluorescent transcriptional reporting of the T cell activation marker Cd69, we defined a classifier for potent versus suboptimal CD69 $^+$  activation states arising from T cell stimulation. In tumors, this delineation provided an additional functional readout among  $T_{EX}$  subsets, marked by enhanced effector molecule production. The more potent Cd69-TFP $^{hi}$  state was the most prominent in a T cell–mediated tumor clearance model, displaying increased engagement and superior tumor cell killing. Simultaneous analysis of gene and protein expression in human head and neck tumors enabled a similar strategy to identify Cd69RNA $^{hi}$ CD69 $^+$  cells with enhanced functional features compared with Cd69RNA $^{lo}$ CD69 $^+$  cells among intratumoral CD8 T cell subsets. Thus, refining the T cell functional landscape in tumors potentiates the identification of rare, potent effectors that could be leveraged for improving cancer treatment.

Copyright © 2025 The Authors, some rights reserved; exclusive licensee American Association for the Advancement of Science. No claim to original U.S. Government Works

#### INTRODUCTION

Within broadly immunosuppressive tumor microenvironments (TMEs), pockets of rare reactive immunity have been discovered, such as those containing conventional type 1 dendritic cells (cDC1s) that support CD8 T cells through antigen presentation (1-4). T cells, which integrate their encounters with antigens over their lifetime (5-7), require potent antigen stimulation for antitumor function. Yet, chronic stimulation by persistent antigen in the TME conversely drives precursor CD8 T cells to dysfunctional or exhausted (T<sub>EX</sub>) states (8), driven by the transcription factor (TF) TOX (9, 10). This undesirable path to T cell exhaustion is increasingly well understood, including its distinct developmental stages (11-13); molecular markers (10, 14-18); and transcriptional, epigenetic (9, 10, 15, 19-21), and microenvironmental drivers (22-25). Although such knowledge has been critical to shape our understanding of T cell dysfunction in tumors, explicit strategies to delineate potent cytotoxic CD8 T cells within this exhausted milieu are not well established.

Tissue-resident memory T cells ( $T_{RM}$  cells) expressing CD69 and/ or CD103 are one possible class of T cells (26, 27) with augmented effector function (28) that might diverge from the lineage of  $T_{EX}$  differentiation. Although cells bearing these markers have been implicated in strong antitumor responses (29, 30), their degree of homogeneity and divergence from exhaustion are not fully understood (28, 31). Efforts to identify potent effector functions under chronic

<sup>1</sup>Department of Pathology, University of California, San Francisco, San Francisco, CA 94143, USA. <sup>2</sup>ImmunoX Initiative, University of California, San Francisco, San Francisco, CA 94143, USA. <sup>3</sup>UCSF CoLabs, University of California, San Francisco, San Francisco, CA 94143, USA. <sup>4</sup>Department of Medicine, University of California, San Francisco, San Francisco, CA 94143, USA. <sup>5</sup>Department of Otolaryngology Head and Neck Surgery, University of California, San Francisco, San Francisco, CA 94143, USA. <sup>6</sup>Department of Anatomy, University of California, San Francisco, San Francisco, CA 94143. USA.

stimulation conditions have led to identification of their TCF1<sup>hi</sup> progenitors and their contribution to responses to immune checkpoint blockade (17, 32, 33). Such progenitor-like CD8 T cells can produce divergent trajectories of  $T_{EX}$  cells, including those biased toward effector-like states (34).

Previous studies have mapped  $T_{\rm EX}$  trajectories that lead to terminally exhausted  $T_{\rm EX}$  ( $T_{\rm EX}$  <sup>Term</sup>), notably identifying intermediates defined by KLR expression ( $T_{\rm EX}$  <sup>KLR</sup>) (12, 13) or associated with better viral control and cytotoxicity (35) and a population of Ly108<sup>-</sup>CD69<sup>-</sup> intermediate  $T_{\rm EX}$  (36) derived and distinct from the progenitor subsets that are Ly108<sup>+</sup> (11) and driven by TCF1 and MYB (17). Such intermediate phenotypes likely also retain some plasticity to be directed away from terminal differentiation (12, 35, 36).

Evidence that effector function may not be fully wired at the onset of T<sub>EX</sub> differentiation derives from studies of key TFs, such as suppression of progenitor-associated factors TCF1 (19) and MYB (17) expression, and overexpression of the AP-1 TFs JUN (37), STAT5A (36), and BATF (38). Down-regulation of early activation gene transcripts including *Jun* and *Nr4a1* occurs in response to stimulation in T and B cells (39, 40). Conversely, AP-1 TF overexpression counteracts the effects of TOX-mediated T cell dysfunction (36, 37).

A key marker related to T cell function is the protein CD69, which has been used both to define T<sub>RM</sub> cell identity and as a marker for early activation. T cells have posttranscriptional regulatory mechanisms for this "early-response" gene, which dissociate its transcription [associated with AP-1 (39, 40) and therefore likely to decrease with repetitive stimulation] from its protein levels (41, 42). This dissociation of RNA and protein, which is broadly known to occur in T and B cells (43, 44), offers an opportunity to study T cell states via comparisons of transcript levels related to history, separate from the CD69 protein levels, indicating recent activation or long-term residency.

Here, we report the generation of a transcriptional reporter of *Cd69* that, together with paired analysis of CD69 protein, provides a different view of the relationships between previous T cell activation history and current capacity as cytotoxic and cytokine-producing effectors. The ability to mark such a dimension of effector states provides

<sup>\*</sup>Corresponding author. Email: matthew.krummel@ucsf.edu

<sup>†</sup>Present address: Department of Cell Biology, Johns Hopkins University, Baltimore, MD, USA.

<sup>‡</sup>Present address: Department of Immunology, University of Texas MD Anderson Cancer Center and James P. Allison Institute, Houston, TX, USA.

an additional layer of functional information beyond that of the established differentiation trajectories of exhaustion.

#### **RESULTS**

## Cd69 transcriptional reporter mice enable tracking of T cell stimulation history in vivo

Although cell surface expression of CD69 has historically been used to indicate both T cell stimulation and tissue retention (45), bioinformatics analysis of multiple datasets showed that transcription of the Cd69 gene is inversely correlated with a history of chronic stimulation. Cd69 mRNA itself is higher in naïve versus effector and early progenitor versus terminally exhausted CD8 T cells (fig. S1, A to C) and in T cells in tumor-adjacent normal areas versus those within paired colorectal [colorectal cancer (CRC)] tumors (fig. S1D). Furthermore, expression of the TFs regulating Cd69 (46) were also differentially higher in naïve versus exhausted CD8 T cells (fig. S1E).

In contrast, CD69 protein expression, driven by T cell receptor (TCR) stimulation or other stimuli such as interferons (IFNs) (47), is often uncoupled from this transcriptional activity as a result of strong 3' untranslated region (3'UTR)–mediated posttranscriptional regulation (41, 42, 48). We thus reasoned that tracking Cd69 RNA alongside its protein might together provide a useful approach to differentiate the potency of activation states in T cells.

To explore this idea, we generated mice in which DNA encoding the teal fluorescent protein (TFP) CreER<sup>T2</sup> and a polyA site was inserted at the 5′ end of the *Cd69* locus (hereafter referred to as *Cd69*-TFP) (Fig. 1A). In lymph nodes of unchallenged *Cd69*-TFP mice, most (~80%; Fig. 1B) of the CD8 T cells were TFP<sup>hi</sup> without expressing surface CD69 protein, as measured by antibody staining (hereafter Q1 or TFP<sup>hi</sup>CD69<sup>-</sup>). We validated that the measured TFP levels reflected *Cd69* RNA expression at steady state (Fig. 1, B and C), consistent with previous studies showing the presence of *Cd69* mRNA that remain translationally repressed until stimulation

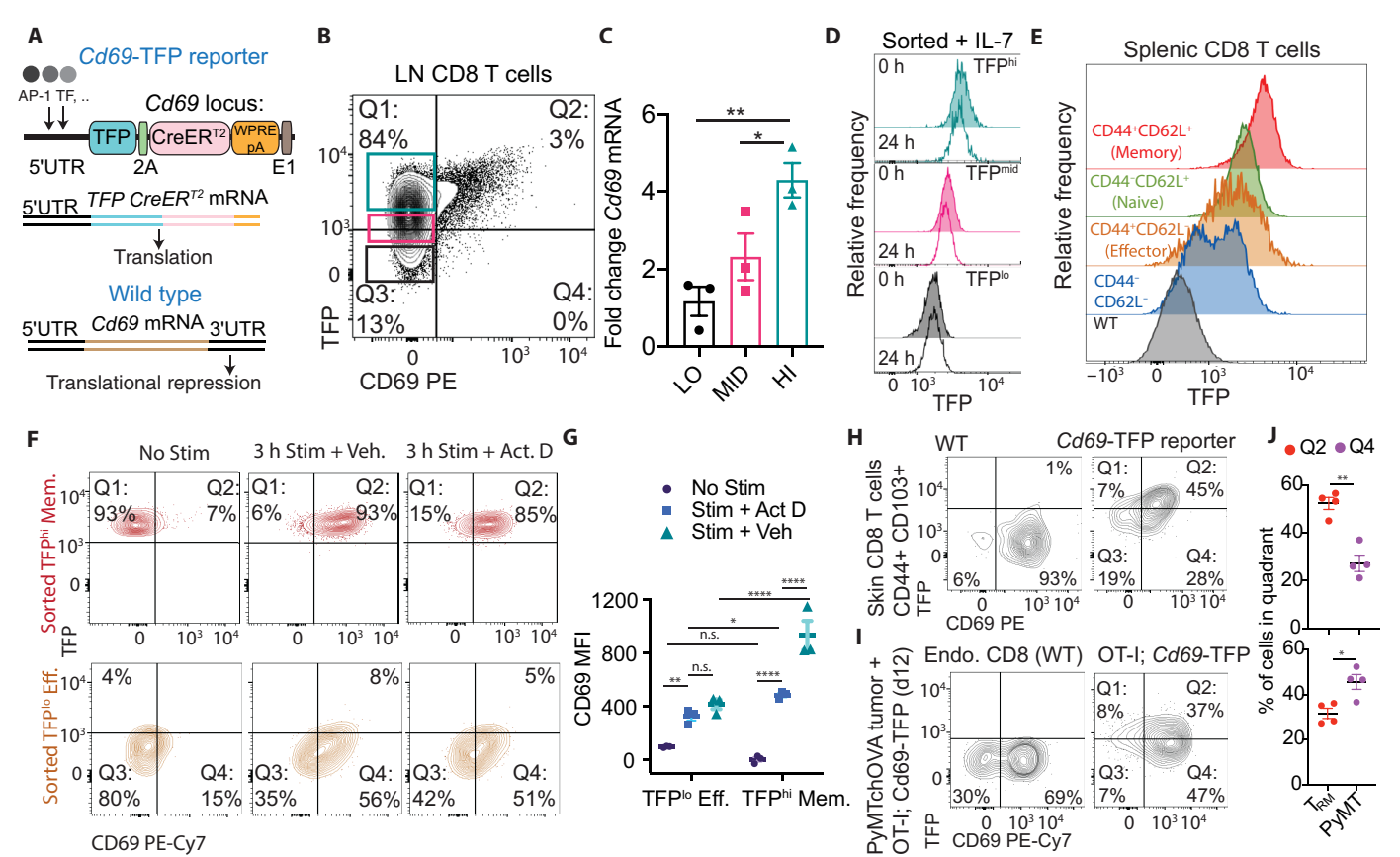


Fig. 1. Distinct expression of *Cd69* transcriptional reporter and CD69 protein in CD8 T cells. (A) Design of the TFP-2A-CreER<sup>T2</sup>-WPRE-pA reporter knocked into the 5'UTR of the *Cd69* locus for transcriptional reporting. (B) TFP and surface CD69 expression in homeostatic LN CD8 T cells; color-coded boxes indicate sorted TFP LO, MID, and HI cell populations assayed for (C) *Cd69* mRNA expression by qPCR. (D) Histograms of TFP expression from sorted TFP<sup>hi</sup> (top 20%), TFP<sup>mid</sup> (middle 30%), and TFP<sup>lo</sup> (bottom 20%) of splenic and lymph node–derived CD8 T cells at 0 and 24 hours postsort, resting in IL-7. (E) Representative histograms of TFP expression in splenic CD8 T cells of different phenotypes (as indicated in the figure panel) from an unchallenged *Cd69*-TFP reporter mouse. (F) Flow cytometry plots of TFP and CD69 in sorted TFP<sup>lo</sup> effector (CD44<sup>+</sup>CD62L<sup>-</sup>) and TFP<sup>hi</sup> memory (CD44<sup>+</sup>CD62L<sup>+</sup>) homeostatic CD8 T cells without stimulation (No Stim), 3-hour αCD3 + αCD28 stimulation + DMSO (3 h Stim + Vehicle), or actinomycin D (5 μg/ml; 3 h Stim + Act. D) and (G) CD69 MFI of the same across conditions. TFP and CD69 expression on (H) skin-resident CD44<sup>+</sup>CD103<sup>+</sup> CD8 T cells in 6-month-old unchallenged WT control and *Cd69*-TFP reporter mice. (I) Endogenous and adoptively transferred OT-I; *Cd69*-TFP reporter CD8 T cells in PyMTchOVA (53) tumors 12 days postadoptive transfer and (J) corresponding quantification of the percentage of cells in Q2 (TFP<sup>hi</sup>CD69<sup>+</sup>) and Q4 (TFP<sup>lo</sup>CD69<sup>+</sup>) states in the same. Plots show means ± SEM. TFP negative gates derived from corresponding WT controls. Null hypothesis testing in (C) and (G) by one-way and two-way ANOVA, respectively, with post hoc Fisher's LSD (least significant difference) and by unpaired *t* test in (J); n = 3 [(C) and (G)] and n = 4 (J) biological replicates representative of at least two independent experiments. \*P < 0.05; \*\*P < 0.005; \*\*P < 0.005; \*\*P < 0.005; \*\*P < 0.005

(42, 49, 50). In addition to this majority population, a small portion of TFPhi CD8 T cells expressed CD69 protein on their cell surfaces (~5%, Q2: TFP<sup>hi</sup>CD69<sup>+</sup>), possibly representing recently stimulated cells, and a third population (~15% Q3: TFPloCD69<sup>-</sup>) was low for both TFP and CD69 (Fig. 1B). Both TFP and CD69 protein levels rose substantially in the context of robust stimulation during the early and intermediate stages of thymic positive selection (fig. S2, A to D) (51) and during the first 3 to 16 hours of stimulation of isolated peripheral CD8 T cells with anti-CD3/CD28 beads (fig. S2G). CD69 protein-positive cells in both of these settings appeared predominantly in the Q2 quadrant (fig. S2, B and D). We found that expression patterns for CD69 protein were similar in reporter and wild-type (WT) mice in both cases (fig. S2, F and I), although surface CD69 levels by mean fluorescence intensity (MFI) were routinely about 50% lower (fig. S2, E and H). These differences were stable when CD8 T cells were sorted by TFP expression and cultured in interleukin-7 (IL-7) overnight, suggesting that they were independent of recent TCR stimulation (Fig. 1D).

In unchallenged mice, TFP expression in CD8 T cells varied with differentiation state. CD44loCD62Lhi naïve cells expressed higher TFP at baseline than CD44<sup>hi</sup>CD62Llo effector CD8 T cells (Fig. 1E). CD44<sup>hi</sup>CD62L<sup>hi</sup> central memory T cells (memory) demonstrated higher levels still, which may be related to higher AP-1 TF activity (52). CD-44loCD62Llo cells expressed the lowest average level of TFP among the populations. When TFPhi memory and TFPho effectors were sorted from unchallenged mice and stimulated with anti-CD3/anti-CD28 beads for 3 hours, TFPhi cells generated more CD69 surface protein as compared with TFPlo cells, an effect also observed in the presence of actinomycin D treatment to block new transcription (Fig. 1, F and G). Both groups maintained their preexisting TFP status during this short stimulation, demonstrating how T cells occupying Q4: TFP<sup>lo</sup>CD69<sup>+</sup> cells may be generated from Q3: TFPloCD69 cells (Fig. 1F). Last, we found that the Q4: TFP<sup>lo</sup>CD69<sup>+</sup> quadrant was modestly represented in skin-resident CD44<sup>+</sup>CD103<sup>+</sup> CD8 T<sub>RM</sub> cells from 6-month-old mice (Fig. 1, H and J) and dominant in ovalbumin (OVA)-specific OT-I T cells in the spontaneous mammary tumors in PyMTchOVA mice (53) 12 days after adoptive transfer (Fig. 1, I and J). The opposite was true for the Q2: TFP<sup>fi</sup>CD69<sup>+</sup> quadrant (higher in T<sub>RM</sub> than tumor cells) (Fig. 1, H to J). Together with our informatic data, this result supported the association between TFP levels and a history of encounters in CD8 T cells.

To further explore this possible relationship of TFPlo cells with a history of repeated stimulation, we set up repetitive "chronic" stimulation cultures using purified CD8 T cells from Cd69-TFP mice. Cells were subjected to three cycles of 48-hour stimulation with 1:1 anti-CD3/anti-CD28 beads, followed by 72-hour rest under either hypoxia (1.5% O<sub>2</sub>) (54) or ambient oxygen levels (normoxia), in the presence of low concentrations of IL-2 after the first cycle (Fig. 2A and fig. S3A). Cd69-driven TFP levels at the end of each cycle were lower than the previous, an effect that culminated in about 50 and 30% reduction under hypoxia and normoxia after three cycles, respectively (Fig. 2, A to C, and fig. S3, A and B). Repeated stimulation concurrently up-regulated exhaustion-associated markers, such as PD1, CD38, and Tim-3, accentuated under hypoxia (54) (Fig. 2F and fig. S3, D and E). Addition of IL-2 without TCR stimulation (fig. S3F) did not induce differentiation (fig. S3G), a decline in TFP expression (fig. S3H), or acquisition of exhaustion-associated markers (fig. S3I). Whereas both Cd69 mRNA (Fig. 2D and fig. S3C) and the upstream AP-1 TF Jun (Fig. 2E) decreased with repeated stimulation, a faster

initial decay was observed when compared with the TFP reporter, likely because of the longer half-life of TFP.

Analyzing the 24-hour time point in each cycle indicated a progressively lower magnitude of reporter expression by MFI from cycle 1 to cycle 3 (fig. S3J), contrasting with CD44, whose peak levels increased in every cycle (Fig. 2A and fig. S3A). However, at 24 hours poststimulation, %TFPhi had reverted to ~100% in each cycle (Fig. 2A). To test whether TFP levels are dependent on the history (cycle number), we further sampled stimulated cells at each cycle at 3-, 6-, and 18-hour time points (Fig. 2G). Both in terms of MFI as well as %TFPhi, we observed progressively lower levels of TFP expression at these intermediate time points (Fig. 2G). Therefore, more stimulation is necessary in later cycles to reach the same levels of TFP, demonstrating the inherent hysteresis in the system.

To test whether low TFP levels reflect different functionality, we sorted TFP<sup>hi</sup> versus TFP<sup>lo</sup> cells from cycle 3-0h and assayed cytokine and granzyme B (GzmB) production after overnight (16 hours) phorbol 12-myristate 13-acetate (PMA)/ionomycin stimulation. A higher proportion of TFP<sup>hi</sup> cells and coexpressed tumor necrosis factor– $\alpha$  (TNF- $\alpha$ ) and IFN- $\gamma$  tended to be positive for GzmB compared with TFP<sup>lo</sup> counterparts (Fig. 2H). A net model based on this set of experiments (Fig. 2I) proposes that, in the CD69:TFP space, trajectories of CD8 T cell state are not retraced during subsequent activation events—rather, TFP levels decrease with repeated stimulation. These experiments suggest that Q2: TFP<sup>hi</sup>CD69<sup>+</sup> cells in this reporter system are T cells that were recently activated yet have not been subject to chronic and exhaustive stimulation.

## Chronic antigen exposure leads to a decline in TFP expression among intratumoral CD8 T cells

To study this reporter in the context of in vivo tumor biology, we adoptively transferred Cd69-TFP reporter-positive OVA-specific CD8 T cells from CD45.1; OT-I TCR transgenic mice into WT mice bearing subcutaneously injected B78chOVA (OVA and mCherry expressed in B78) tumors (Fig. 3A). B78 is an amelanotic B16 variant, which we have previously described as unresponsive to OT-I treatment where adopted T cells are progressively rendered dysfunctional in the tumor (22). Recovered OT-Is from these tumors were ~90% PD1<sup>+</sup> CD44<sup>+</sup> (fig. S4A) and largely found in Q1 and Q2 of the reporter system on the first day they were detected [day 4 (d4)] (Fig. 3B). Although we found low levels of CD69<sup>+</sup> among recently arrived T cells, consistent with the required down-regulation of CD69 to emigrate from the draining lymph node (dLN) (55), by d6 to d7, ~70% of cells were TFPhiCD69+ (Q2; Fig. 3, B and D). By d14, recovered cells were dominantly TFPloCD69 (Q3) and TFPloCD69 (Q4) (Fig. 3, B and D). Consistent with our previous work using this (22) and other models (53), this shift to TFPlo states was accompanied with increased differentiation toward chronic stimulation-driven exhaustion, here measured by PD1<sup>+</sup>CD38<sup>+</sup> (15, 22) among OT-Is (fig. S4B), which also tracked with TOX<sup>hi</sup>TCF7<sup>lo</sup> phenotypes (fig. S4C). Similar trends in intratumoral OT-Is were observed in a spontaneous breast carcinoma tumor model (PyMTchOVA) (53) with adoptive transfer, albeit with a less prominent transient increase in Q2 (fig. S4, D to F).

When the dLN was analyzed, in contrast with the tumor, we found that the vast majority of cells remained TFP<sup>hi</sup> throughout the experiment (Fig. 3, C and E), suggesting that the observed changes relied on the TME. To address the role of the TME more directly, we

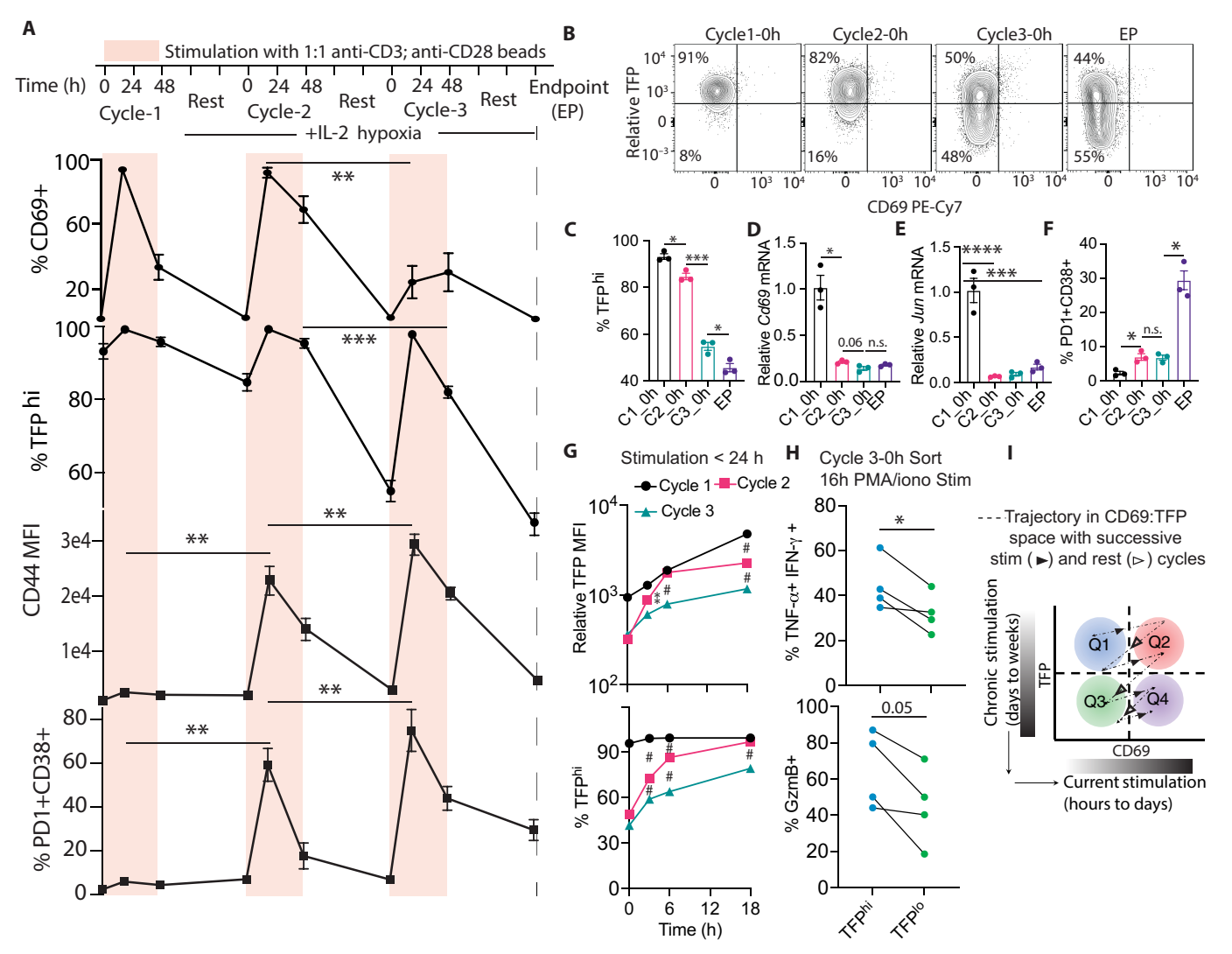


**Fig. 2.** Repeated TCR stimulation suppresses *Cd69* transcription and the reporter TFP in CD8 T cells. (A) %CD69<sup>+</sup>, %TFP<sup>hi</sup>, CD44 MFI, and %PD1<sup>+</sup>CD38<sup>+</sup> of freshly isolated CD8 T cells through successive cycles of 48-hour stimulation and 72-hour resting in hypoxia + IL-2 (*n* = 3 biological replicates. (**B**) Representative flow cytometry plots showing relative TFP (TFP normalized to WT control) and CD69 expression at the beginning of cycles 1, 2, and 3 and end point (EP). (**C**) %TFP<sup>hi</sup>, (**D**) *Cd69* mRNA and (**E**) *Jun* mRNA by qPCR, and (**F**) %PD1<sup>+</sup>CD38<sup>+</sup> at the same time points. (**G**) TFP expression by MFI and %TFP<sup>hi</sup> with 0-, 3-, 6-, and 18-hour stimulation at cycle 1, 2, and 3. (**H**) Cytokine and GzmB expression in sorted TFP<sup>hi</sup> and TFP<sup>lo</sup> cells from the cycle 3-0h condition restimulated 16 hours with PMA/ionomycin. (**I**) Schematic showing the trajectory of CD8 T cells within the TFP:CD69 states (quadrants) with successive stimulation and rest, providing a reading of the history of stimulation (color gradients represent chronic and current stimulation levels). Null hypothesis testing by one-way ANOVA with Tukey's post hoc test [(A) and (C) to (F)] and two-way ANOVA with Tukey's test post hoc in (G) comparing between pairwise cycles at the same time point, paired *t* tests in (H). \**P* < 0.05; \*\**P* < 0.01; \*\*\*\**P* < 0.001; \*\*\*\*\**P* < 0.0001; n.s., not significant; #*P* < 0.001 in (G).

modified a tumor slice overlay protocol (*56*) where a selection of T cells encountered the isolated TME at the same time (Fig. 3F). In this setting, the progression of phenotypes through CD69:TFP quadrants (Fig. 3G and fig. S5A) and the acquisition of exhaustion markers (fig. S5, B to D) recapitulated in vivo data. Slice cultures also allowed analysis of proliferation in the slice-infiltrating OT-I T cells over time using violet proliferation dye (VPD) (fig. S5E). VPD dilution accompanied the general decrease in TFP expression with each division, exemplified at d3 (fig. S5F). Q4 cells at d8 had undergone more division (fig. S5G) and were more PD1<sup>+</sup>CD38<sup>+</sup> than those from Q2 (fig. S5H), suggesting that they were further along the T<sub>EX</sub> differentiation trajectory. Analyzing the level of VPD within

cells in the four CD69:TFP quadrants at each time point reinforced the trajectory of transition from TFP $^{\rm hi}$ Q1 and Q2 states to TFP $^{\rm lo}$ Q3 and Q4 states (fig. S5I).

To further assess the conversion of T cells among these CD69:TFP states in the context of tumors, we sorted OT-Is d12 posttransfer by their CD69:TFP phenotypes from B78chOVA tumors (Q2 to Q4) and the dLN (Q1), restimulated these cells in vitro with anti-CD3/CD28 beads, and tracked the resultant quadrant transitions after 3 days (Fig. 3, H and I). Q1 cells transitioned to Q1 and Q2 and partially to Q3, whereas Q2 converted to Q2 and Q4, with small percentages in Q1 and Q3 (Fig. 3, H and I). Sorted Q3 and Q4 cells both remained predominantly (~70 to 80%) within the Q3 and Q4 states,

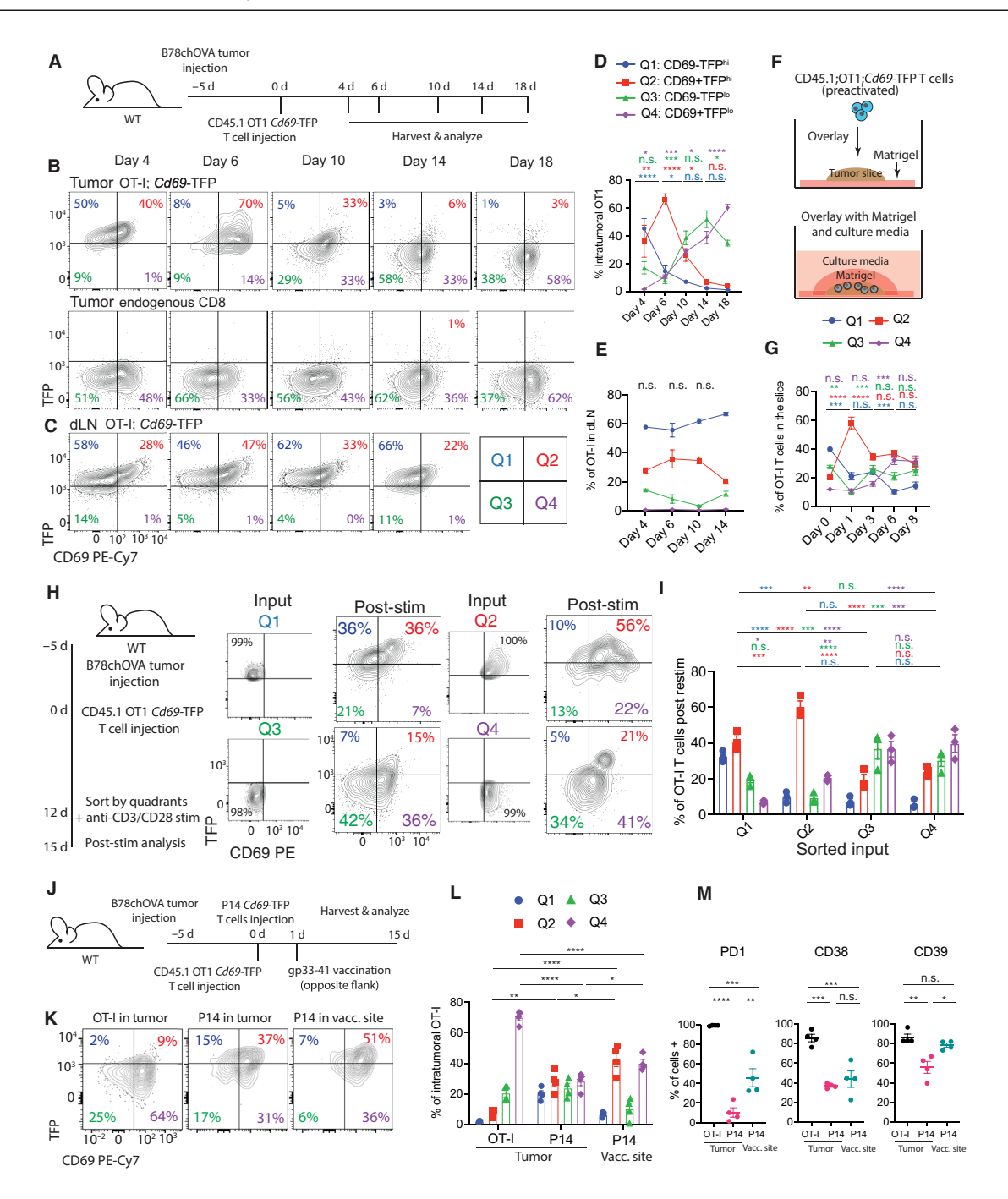


Fig. 3. Chronic antigen exposure in tumors leads to a decline in TFP expression in CD8 T cells. (A) Experimental schematic to track antigen-specific T cells in B78chO-VA tumors over time. d, days. Flow cytometry plots showing TFP and CD69 expression of (B) adoptively transferred OT-IT cells and endogenous CD8 T cells in the (D) tumor and (C) OT-IT cells in corresponding tumor-dLNs over time. Corresponding CD69:TFP quadrant (Q1 to Q4) distribution for the same OT-IT cells in the (D) tumor and (E) tdLN. (F) Schematic representation of long-term tumor slice culture setup; preactivated: 48-hour stimulation with αCD3 + αCD28 followed by 48-hour rest in IL-2. (G) CD69:TFP quadrant distribution of slice-infiltrating OT-IT cells over time. (H) Representative flow cytometry plots and (I) quantification of resultant quadrant distribution of OT-IT cells sorted by their Cd69:TFP quadrants from B78chOVA tumors (Q2 to Q4) or dLN (Q1) 12 days postadoptive transfer and restimulated with anti-CD3/anti-CD28 for 3 days. (J) Experimental schematic of tumor injection and contralateral vaccination with distinct antigen specificities (OT-I and P14; P14 cells are 20 to 25% less TFP+ than OT-Is at baseline before injection). (K) Flow cytometry plots showing TFP and CD69 profiles of OT-I, P14 T cells in the OVA+ tumor and P14 T cells at the gp33-41 vaccination (vacc.) site. (L) CD69:TFP quadrant distribution of the same and (M) PD1, CD38, and CD39 expression among the same three groups. Representative data from two or three independent experiments; three to five mice; or five or six slices, time points, or experiments. Preslice overlay samples in duplicate. Plots show means ± SEM. \*P < 0.05, \*\*P < 0.01, \*\*\*P < 0.01, \*\*\*P < 0.01, and \*\*\*\*P < 0.001 and \*\*\*\*P < 0.0001 for null hypothesis testing using one-way ANOVA for each quadrant with selected pairwise multiple comparisons between time points using the post hoc Holm-Šidák test in (D), (E), and one-way ANOVA with Tukey's post hoc test in (M).

suggesting a propensity to interconvert between these states (Fig. 3, H and I). Of note, both Q3 and Q4 cells retained some ability to convert to TFP<sup>hi</sup> Q2 upon strong stimulation, although this propensity was substantially lower than those of Q1 and Q2 cells (Fig. 3, H and I).

To determine how this progression from TFPhi to TFPlo states is related to antigen stimulation and the corresponding microenvironment, we isolated CD8 T cells with a nontumoral specificity [lymphocytic choriomeningitis virus (LCMV)-specific P14; Cd69-TFP] and assessed their state both within a tumor that did not express their antigen and within a vaccination site, as compared with OT-I T cells from an OVA-expressing tumor (Fig. 3J). When the P14; Cd69-TFP cells were coinjected with CD45.1; OT-I; Cd69-TFP T cells into B78chOVA tumor-bearing mice that then received a priming gp33-41 peptide vaccination distal to the tumor (Fig. 3J), we found that they expressed higher TFP levels in the tumor than OT-Is (Fig. 3, K and L). P14 T cells at the contralateral vaccination site also remained substantially TFPhi with a five times increase in the frequency of Q2 cells (Fig. 3, K and L) compared with tumor OT-Is. These differences in CD69:TFP quadrant distributions aligned with the expression of surface markers PD1, CD38, and CD39, which are associated with exhaustion (Fig. 3M). Overall, these surface proteins were highest in the intratumoral OT-Is, intermediate in the P14s at the vaccination site, and comparatively low in the nonspecific intratumoral P14s (Fig. 3M). Hence, exposure to the TME alone did not lead to loss of a Q2 state, and presentation of antigen at a different site also did not lead to decreases in TFP level. Overall, these data support that chronic antigen-specific stimulation of T cells specifically in a TME can drive a TFP<sup>lo</sup>CD69<sup>+</sup> (Q4) phenotype.

## TFP<sup>hi</sup>CD69<sup>+</sup> (Q2) marks a state of relative functional potency in intratumoral T<sub>EX</sub> cells

We next sought to establish whether Q4 and Q2 cells were also functionally different and determine how this related to  $T_{\rm EX}$  cell differentiation in tumors, as highlighted in single-cell sequencing (12, 57, 58). We thus pooled OT-I; Cd69-TFP T cells from eight B78chOVA tumors 12 days after adoptive transfer, sorted for CD69:TFP quadrants, barcoded each population separately, and performed single-cell RNA sequencing (scSeq) (Fig. 4A). From 13,352 cells, nine computationally derived clusters were identified (Fig. 4B), driven largely by previously identified canonical markers and with similar predicted differentiation trajectories (fig. S6, A to C). Strong associations were observed between the gene expression patterns corresponding to  $T_{\rm EX}^{\rm Prog}$ ,  $T_{\rm EX}^{\rm E.E.ff}$ ,  $T_{\rm EX}^{\rm Term}$ ,  $T_{\rm EX}^{\rm ISG}$ , and  $T_{\rm EX}^{\rm KLR}$  subsets in our dataset and those that previously established this nomenclature (12) (fig. S6E). Some differences exist, such as in the  $T_{\rm EX}^{\rm Int.}$  and  $T_{\rm EX}^{\rm Mem}$  subsets, and may be attributable to variability between tumor-derived subsets here and prior LCMV-derived ones.

Barcoding of sorted cells by CD69:TFP states allowed mapping of quadrant distributions of these post– $T_{\rm EX}$  cell subsets (12) (Fig. 4, B and C, and fig. S6D).  $T_{\rm EX}^{\rm Prog}$  cells were barcoded as coming from Q1 or Q2 states, and more terminally differentiated subsets of  $T_{\rm EX}^{\rm Int}$ ,  $T_{\rm EX}^{\rm Term}$  were predominantly derived from Q3 and Q4 barcoded cells (Fig. 4C).  $T_{\rm EX}^{\rm KLR~Eff}$ , previously the most likely candidates to have high effector function, were heterogeneous, expressing barcodes indicative of either Q2 or Q4.

Using flow cytometry to mark the differentiation trajectory similarly, we found that progenitor (TCF1<sup>+</sup>) OT-I cells were predominantly associated with Q1 and Q2, putative "effectors" (CD94<sup>+</sup>:

CD94 or KLRD1 is the gene product of Klrd1, one of the markers of the T<sub>EX</sub> KLR Eff subset) predominantly were Q2 and Q4 (with Q2 > Q4), and "exhausted" (PD1+CD38+) cells were enriched in Q4 and Q2 (Q4 > Q2) (Fig. 4, D to F), trends also recapitulated in spontaneous mammary PyMTChOVA tumors (fig. S7, A to C). The distribution of key TF and other canonical marker expression also supported this broad relationship between T cell differentiation and CD69:TFP distributions (Fig. 4G). Transcripts for progenitor markers primarily concentrated in Q1, with AP-1 factors in Q1 and Q2, whereas exhaustion-related markers largely occupied Q3 and Q4 states. Effector lineage and function-associated Batf, Tbx21, and If ng were highest in Q2 (Q2 > Q4), along with signatures of noncanonical enhanced effectors derived from STAT5A overexpression (36) or MYB knockout (KO) (17) (Fig. 4G). T<sub>RM</sub> markers Prdm1 and Id2 (27) tended to be higher in TFPlo Q4 than TFPhi Q2 in this context (Fig. 4G). A core tissue residency signature (59) was split between Q2 and Q4 (Q2 > Q4) (fig. S6F), whereas an orthogonal circulatory gene signature (59) was concentrated in Q1 and Q2 (fig. S6F). Identifying T<sub>RM</sub>-like cells by CD103 and CD69 expression by flow cytometry, we found their relative abundances in the Q2 and Q4 states to be similar (fig. S6G), although the frequency of such cells among intratumoral OT-Is in this relatively short time of residence was only around 1% on average (fig. S6H). A gene signature associated with checkpoint blockade-associated CD101<sup>-</sup>Tim3<sup>+</sup> transitory effectors was highest in Q2 and that of its CD101<sup>+</sup>Tim3<sup>+</sup> terminally exhausted counterpart (13) was highest in Q4 followed by Q3 (Fig. 4G).

Within all OT-I cells, we found enhanced expression of the intracellular cytokines TNF- $\alpha$ , IFN- $\gamma$ , and cytotoxicity-associated GzmB in intratumoral Q2 cells as compared with their Q4 counterparts, both after restimulation postsorting (Fig. 4, H and I, and fig. S7D) and at baseline (Fig. 4J and fig. S7, F and G). Q1 cells were comparably cytokine- and granzyme-positive upon restimulation as Q2, whereas Q3 cells were similarly less responsive as Q4 (Fig. 4I and fig. S7D). Without restimulation, Q2 cells produced more cytokine and granzyme than Q1 cells, and the same was true for Q4 and Q3 cells (fig. S7E). We next interrogated Q2 as compared with Q4 cells from distinct differentiation states to determine whether there were variations in functional potency within each given classification. We gated further on subsets that were split between the Q2 and Q4 states, namely, an early progenitor Ly108<sup>+</sup>CD69<sup>+</sup> (11) (56% Q2 and 44% Q4; Fig. 4K), effector-like CD94+ (33% Q2 and 46% Q4; Fig. 4L), and terminal exhaustion-like PD1<sup>+</sup>CD38<sup>+</sup> (23% Q2 and 53% Q4; Fig. 4M) subsets, appearing at different junctures of the T<sub>EX</sub> differentiation trajectory. Within the Ly108<sup>+</sup>CD69<sup>+</sup> (Fig. 4K) subset, cells in the Q2 state produced more TNF-α and IFN-γ (but not GzmB) than those in Q4. Of note, a second progenitor Ly108<sup>+</sup>CD69<sup>-</sup> population (11), split between Q1 and Q3, showed no significant difference between Q1 and Q3 in the same metrics (fig. S7H). Furthermore, within CD94<sup>+</sup> (Fig. 4L) and PD1<sup>+</sup>CD38<sup>+</sup> subsets (Fig. 4M), cells in the Q2 state consistently showed higher expression of these cytotoxic molecules in most cases than the Q4 counterparts. The Ly108<sup>-</sup>CD69<sup>+</sup> terminal subset aligned with the PD1<sup>+</sup>CD38<sup>+</sup> subset (fig. S7I) and therefore demonstrated similar Q2 versus Q4 differences in cytokine and granzyme expression (fig. S7J). Thus, this delineation of Cd69 transcription (by TFP) among CD69<sup>+</sup> cells provides an additional layer indicative of relative functionality of CD8 T cells beyond the established trajectory of an intratumoral  $T_{EX}$  differentiation landscape.

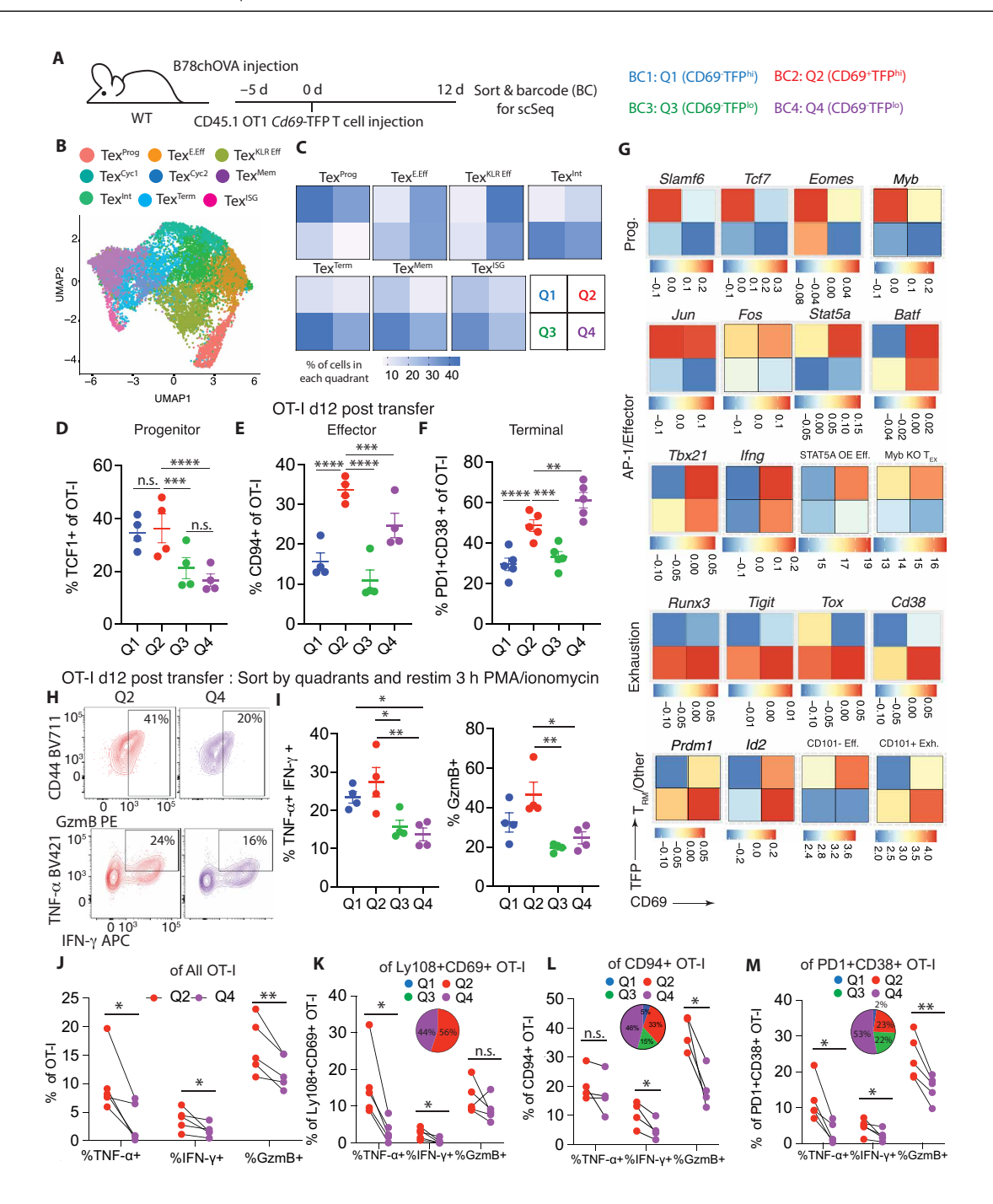
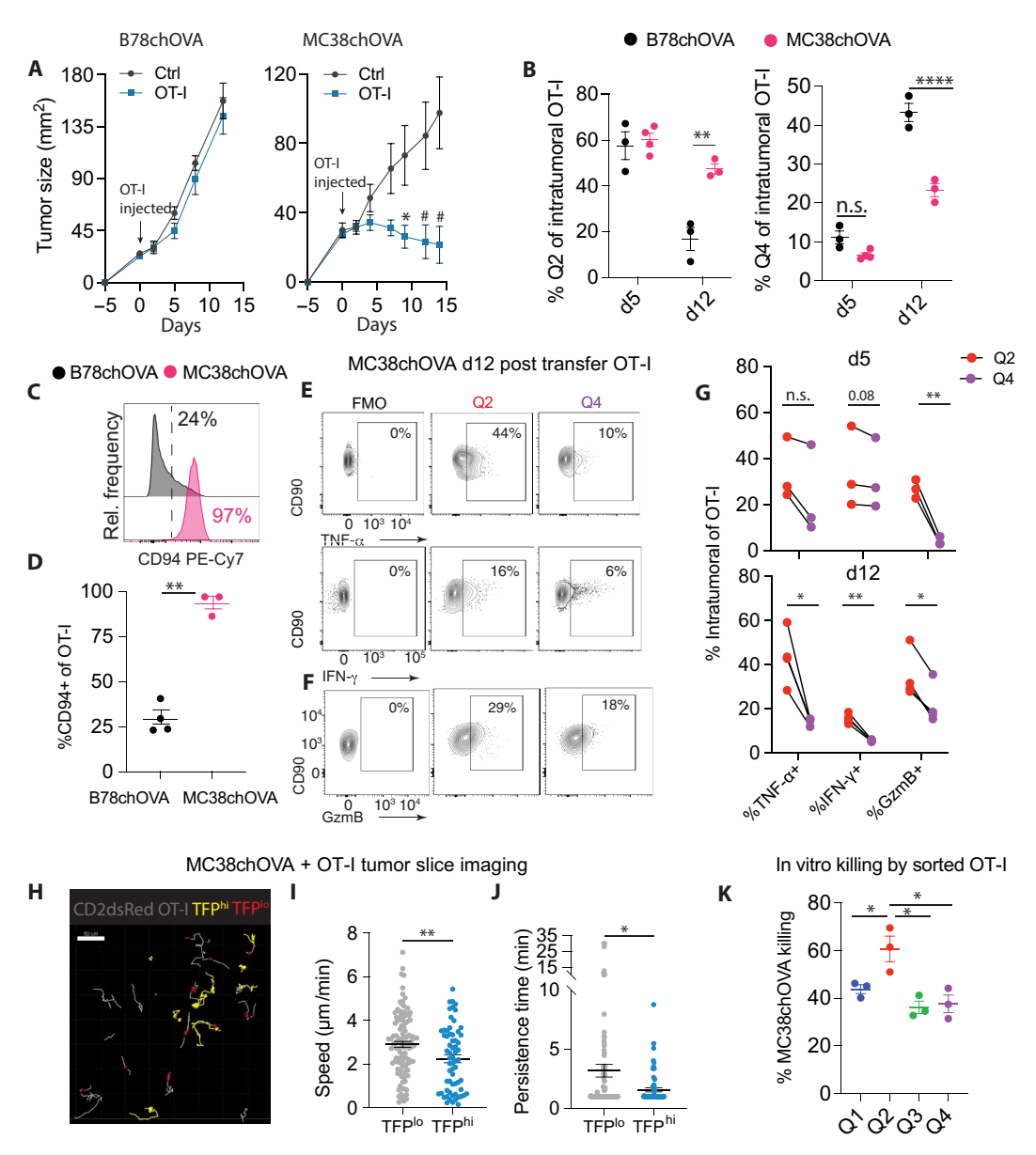


Fig. 4. TFP<sup>hi</sup>CD69<sup>+</sup> (Q2) marks a potent functional state of antigen-specific CD8 T cells within tumors. (A) Experimental schematic for single-cell transcriptomic profiling of intratumoral OT-I T cells sorted by CD69:TFP quadrants. (B) Uniform Manifold Approximation and Projection (UMAP) representation of the scSeq data color-coded by computationally derived clusters. (C) Heatmap showing the percentage of cells that belong to the four CD69:TFP quadrants Q1 to Q4 within each cluster. Distribution of the percentage of cells bearing (D) progenitor (TCF1<sup>+</sup>), (E) effector (KLRD1 or CD94<sup>+</sup>), or (F) terminal exhaustion (PD1<sup>+</sup>CD38<sup>+</sup>) markers within each CD69:TFP quadrant. (G) Heatmaps (color scale represents normalized mRNA expression) showing the distribution of transcripts (canonical progenitor, AP-1/effector, exhaustion, and tissue-resident memory-related genes) and transcriptomic signatures [corresponding to Stat5a overexpressing effectors (36), Myb KO (17), CD101<sup>-</sup>Tim3<sup>+</sup>, and CD101<sup>+</sup>Tim3<sup>+</sup> (13) exhausted CD8 T cells] in the four CD69:TFP quadrants. (H) Flow cytometry plots showing representative GzmB and cytokine expression in Q2 versus Q4 intratumoral OT-Is from B78chOVA tumors 12 days postadoptive transfer, which were sorted and then restimulated for 3 hours in PMA/ionomycin, and (I) corresponding bar graph quantification of the same. (J) Cytokine and GzmB expression in intratumoral OT-I T cells at baseline (d12 postadoptive transfer) in the Q2 versus Q4 activation state. Cytokine and GzmB expression of Q2 versus Q4 OT-I T cells within (K) Ly108<sup>+</sup>CD69<sup>+</sup> (11), (L) CD94<sup>+</sup>, and (M) PD1<sup>+</sup>CD38<sup>+</sup> intratumoral OT-I subsets with the inset pie chart showing the percentage of cells in each quadrant within the corresponding subsets. Bar plots show means ± SEM. \*P < 0.05, \*\*P < 0.01, \*\*\*P < 0.001, \*\*\*P < 0.001, \*\*\*P < 0.001 for null hypothesis testing by ratio paired t test [(J) to (M); regular paired t tests used where the ratio test was undefined because of at least one data point being zero] and repeated-m

## TFP<sup>hi</sup>CD69<sup>+</sup> (Q2) CD8 T cells display increased functionality during tumor regression

We next asked whether CD8 T cells in this Q2 activation state would be more prominent during a productive antitumor response such as T cell–mediated tumor control. To do this, we investigated subcutaneously injected MC38chOVA [MC38 CRC cell line modified with the same chOVA construct as PyMTchOVA (53) and B78chOVA] tumors that are actively controlled in response to the adoptive transfer of

OVA-specific OT-I T cells, whereas B78chOVA are not (Fig. 5A). *Cd69*-TFP;OT-I T cells in regressing MC38chOVA tumors retained their predominantly Q2 (TFP<sup>hi</sup>CD69<sup>+</sup>) phenotype even at d12 post-adoptive transfer, in contrast with those in the growing B78chOVA tumors (Fig. 5B and fig. S8A). Conversely, the chronic activation-induced Q4 (TFP<sup>lo</sup>CD69<sup>+</sup>) subset was less prominent in MC38chOVA compared with B78chOVA (Fig. 5B). However, the relatively high TFP<sup>hi</sup> proportion (at least 60% at all time points) in the corresponding



**Fig. 5. TFP**<sup>hi</sup>**CD69**<sup>+</sup> **(Q2) CD8 T cells display increased functionality during tumor regression. (A)** Tumor growth curves of B78chOVA and MC38chOVA with and without OT-I transfer 5 days after tumor injection, as indicated by arrows (n = 4 or 5 per group). **(B)** Quantification of the percentage of Q2 and Q4 cells at d5 and d12 postadoptive transfer in the two tumor models. **(C)** Typical CD94 expression in intratumoral OT-Is in B78chOVA and MC38chOVA tumors d12 postadoptive transfer and **(D)** corresponding quantification. **(E to G)** Flow cytometry plots showing (E) intracellular cytokine and (F) GzmB expression in OT-IT cells in the Q2 versus Q4 state d12 postadoptive transfer in MC38chOVA tumors and (G) quantification of the same at d5 and d12. **(H)** Representative tumor slice image showing cell migration tracks associated with TFP<sup>lo</sup> (red) and TFP<sup>hi</sup> (yellow) CD2dsRed;OT-IT cells and corresponding quantification of **(I)** cell speed and **(J)** persistence of migration. **(K)** In vitro killing of MC38chOVA cells by OT-IT cells sorted by CD69:TFP quadrants from MC38chOVA tumors 8 days after adoptive transfer. Bar plots show means  $\pm$  SEM; \*P < 0.05, \*\*P < 0.01, \*P < 0.001, and \*\*\*\*P < 0.0001 for null hypothesis testing two-way ANOVA with post hoc Šidák's test for comparisons among treatments/tumor models in **(A)** and **(B)**, unpaired t test t (C), (I), and (J), ratio paired t tests (G), and repeated-measures one-way ANOVA with post hoc Holm-Šidák test (K).

dLNs was similar in both [MC38chOVA (fig. S8B) and B78chOVA (Fig. 2, C and D)].

From d5 to d12, transferred OT-Is in MC38chOVA tumors showed a decline in Ly108 expression and a concomitant increase in exhaustion-associated coexpression of PD1 and CD38, although the percentage of the latter was lower than that in B78chOVA [MC38hOVA (fig. S8C) and B78chOVA (fig. S4B)]. Further investigation revealed the OT-I cells in the MC38chOVA tumors were ~80% CD94 (KLRD1)<sup>+</sup> at d5, which rose to >90% at d12 (fig. S8C). This was significantly higher compared with about 25% in the B78chOVA model (Fig. 5, C and D), indicating a dominant KLR-effector phenotype in the MC38chOVA (35). Once again, the CD103<sup>+</sup> subset of the transferred OT-Is was only around 1% (fig. S8C), therefore ruling out  $T_{RM}$ -like cells as the dominant potent effectors in this context. Among these largely CD94<sup>+</sup> OT-I T cells in MC38chOVA, those in the Q2 state again tended to express higher levels of TNF-α and IFN-γ and GzmB than Q4 counterparts (Fig. 5, E to G). These trends were already prevalent at d5 but showed a stronger divergence of phenotypes at d12 (Fig. 5G). Further evidence of in situ functional engagement of TFP<sup>hi</sup> cells was obtained by live two-photon microscopy where those cells could be identified by analysis of TFP levels over non-TFP controls (fig. S8D). This analysis demonstrated enhanced cell arrest of the TFPhi (mostly ~75% Q2) cells within MC38chOVA tumor slices harboring adopted OT-Is, with lower speed (Fig. 5, H and I), directional persistence (Fig. 5J), and overall motility (fig. S8E). In both mouse (60) and human (56) tumors, these features are associated with lower levels of exhaustion. In addition, among the OT-I cells sorted from MC38chOVA tumors by CD69:TFP quadrants, those in the Q2 state also showed the highest killing capacity when exposed to MC38chOVA cells in vitro (Fig. 5K). These data support the use of TFP and CD69 to mark a potent activation state of intratumoral CD8 T cells in mice.

## Demarcation of *Cd69* RNA levels enables functional delineation of exhausted T cell subsets in head and neck squamous cell carcinoma

We next sought to independently identify similar CD8 T cell activation states in human tumors using multimodal CITE-Seq (cellular indexing of transcriptomes and epitopes by sequencing) on CD45<sup>+</sup> enriched cells to analyze tumor biopsies from patients with head and neck squamous cell carcinoma (HNSC) (Fig. 6A). Within tumorderived cell populations initially from a pooled sample of two patients, we gated on CD8 T cells using antibody-tagged markers (fig. S9A), and simultaneous readouts of Cd69 mRNA and surface CD69 protein expression allowed CD8 T cells to be gated into four quadrants (fig. S9B). Unbiased combined protein-RNA-driven weighted nearest neighbor determination grouped CD8 T cells into seven major clusters and two minor, atypical clusters (MT<sup>+</sup> and CXCL2<sup>+</sup>) (Fig. 6B). On the basis of the differentially expressed genes (DEGs) and overlaying exhaustion and naïve markers (Fig. 6C), we identified one naïve (Tn), one memory (Tem), and five exhaustion-associated clusters, including a proliferative and a CXCL13<sup>+</sup> subset (Fig. 6B and fig. S9, C and D). In contrast with the naïve and exhaustion scores, expression of progenitor- and effector-associated genes previously identified in chronic infection in mice (12) revealed diffuse expression in the major clusters (fig. S9E). This may be expected because the trajectory of differentiation and typical subset identities in human tumors are not identical to the  $T_{EX}$ differentiation trajectories in mice. Therefore, we used scSeq data corresponding to a recently published pan-cancer human CD8 T cell atlas

(61) and overlaid the DEGs for each major cluster in our dataset onto the established nomenclatures in the published atlas (fig. S9, F and G). This analysis supported the classification of the five  $T_{\rm EX}$  clusters as early, intermediate or "int," late, cycling or "cyc," and CXCL13, whereas Tn and Tem signatures corresponded directly to naïve and memory clusters in the atlas (fig. S9G). As in mice, Q2 (Cd69RNA  $^{\rm hi}$ CD69protein  $^{+}$ ) and Q4 (Cd69RNA  $^{\rm lo}$ CD69protein  $^{+}$ ) states in this human tumor sample also spanned several clusters (Fig. 6D). A majority of the exhausted CD8 T cells existed in the Q4 state, as indicated by the coincidence of the exhaustion score (based on protein expression) and the Q4 cells (Fig. 6, C and D). Representation of the Q2 state was skewed toward the Tn, Tem, and  $T_{\rm EX}^{\rm Early}$  and that of Q4 toward the  $T_{\rm EX}^{\rm Late}$ ,  $T_{\rm EX}^{\rm CXCL13}$  subsets and the  $T_{\rm EX}^{\rm Int}$  cluster (Fig. 6E).

Having classified both the T<sub>EX</sub> cell subsets and the Q1 to Q4 quadrants within these intratumoral CD8 T cells, we then investigated the patterns of functional gene expression between the Q2 and Q4 states. Using the CITE-Seq data in a patient-by-patient analysis for a total of seven patients (fig. S9H), we found that Q2 cells expressed higher levels of the AP-1 TFs Jun and FOS (Fig. 6F). Enhanced expression of IFNG and a decreased exhaustion score in Q2 compared with Q4 cells (Fig. 6G) indicated similar, functionally divergent activation states, mirroring those elucidated in mice. As in the murine scSeq data, T<sub>RM</sub>-like cells delineated by CD103 protein expression were represented both in Q2 and Q4 states (fig. S9I). We next interrogated the features of this delineation within the  $T_{\text{EX}}^{\phantom{\text{Early}}}$ and T<sub>EX</sub> cell subsets, with sufficient representation (using a threshold of 50 cells in a given subgroup) in three and four patients, respectively, as biological replicates. Even within these distinct T<sub>EX</sub> cell subsets, the same trends of enhanced Jun and IFNG expression and decreased exhaustion were observed (Fig. 6G), indicating a similar axis of effector function beyond the T<sub>EX</sub> differentiation trajectory.

## A *CD69*<sup>hi</sup>CD69<sup>hi</sup> (Q2) transcriptomic signature is associated with antitumor effector function across human cancers

To the extent that transcriptomic signatures can capture the multimodal delineation of T cell state offered by our reporter and CITE-Seq, these are useful in their applicability to existing transcriptomic data on human tumors. With this objective, we identified DEGs between Q2 and Q4 states from CITE-Seq. The Q2 signature included not only CD69 but also its upstream TFs, Jun, FOS, and NR4A1, whereas the Q4 signature largely comprised actin-related genes and CD74 (Fig. 7A). We then overlaid the expression of the Q2 and Q4 gene signatures onto the pan-cancer CD8 T cell atlas described above (61) (Fig. 7B). We arranged the well-represented clusters in decreasing order of the naïve gene expression score (SELL, IL7R, TCF7, LEF1, and CCR7) (Fig. 7C). As expected, the exhaustion gene expression score [gene list as previously described (62)] in the same clusters displayed approximately the opposite (increasing) order (Fig. 7C). The Q2 score was prominent in the intermediate natural killer-like CD8 T cells expressing effector markers, whereas the Q4 signature associated highly with GZMK- and CXCL13-expressing  $T_{EX}$  cell subsets (Fig. 7C).

We also included previously identified  $T_{EX}$  cell subsets in addition to our CD69 RNA-based delineations in this analysis. Transcriptomic signatures reported for phenotypically opposing Ly108<sup>+</sup>CD69<sup>+</sup> versus Ly108<sup>-</sup>CD69<sup>+</sup> (11) and CD101<sup>-</sup>Tim3<sup>+</sup> versus CD101<sup>+</sup>Tim3<sup>+</sup> subsets (13) using human ortholog genes were examined. Cell-by-cell expression of Ly108<sup>-</sup>CD69<sup>+</sup> and CD101<sup>+</sup>Tim3<sup>+</sup> signatures (both associated with terminal exhaustion) moderately correlated with each other

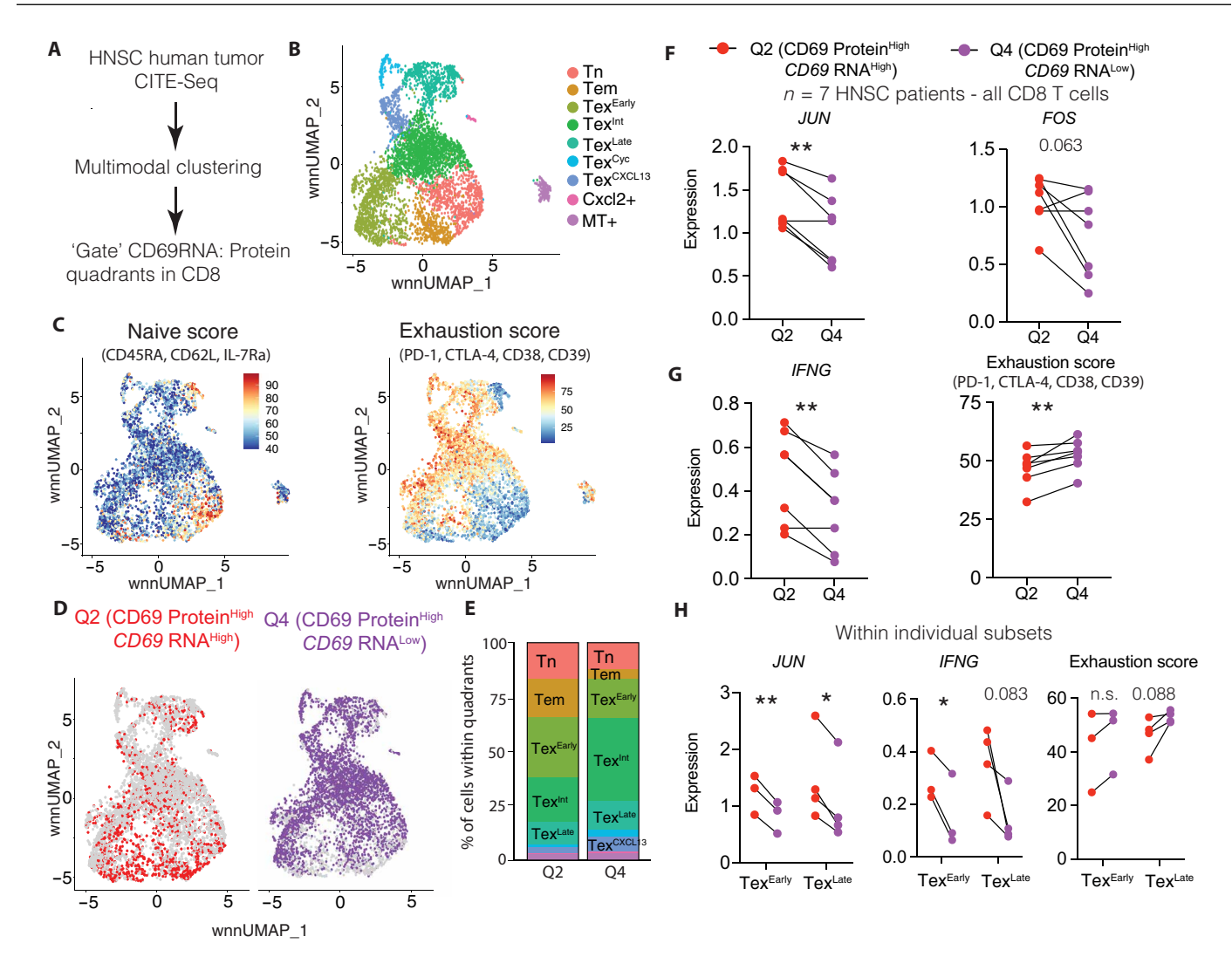


Fig. 6. Simultaneous analysis of *CD69* RNA and protein expression by CITE-Seq delineates intratumoral CD8 T cell activation states in head and neck squamous cell carcinoma. (A) Schematic description of human HNSC tumor CITE-Seq analysis. (B) UMAP showing weighted nearest neighbor (WNN)—determined clusters by multimodal RNA and protein analysis of 5002 CD8 T cells from pooled sequencing of biopsies from two patients. (C) Overlay of naïve and exhaustion score and (D) that of Q2 and Q4 cells (determined by gating on CD69 protein and RNA) on the same WNN-UMAP. (E) Stacked bar plot showing the relative contribution of the various subsets to the Q2 and Q4 states, as defined by *CD69* RNA and CD69 surface protein. Patient-by-patient expression of (F) *JUN* and *FOS*; (G) *IFNG* and exhaustion markers in Q2 and Q4 CD8 T cells; and (H) *JUN*, *IFNG*, and exhaustion markers between Q2 and Q4 within individual  $T_{EX}^{Early}$  and  $T_{EX}^{Early}$  subsets. \*P < 0.05; \*\*P < 0.01; n.s., not significant by paired t tests [(F) to (H)], P = T patients in (F) and (G) and P = T or 4 in (H).

(rho = 0.48) (fig. S10C). The Q4 signature showed weaker (rho = 0.27, 0.25) correlation with both aforementioned signatures, whereas Q2 was largely uncorrelated with all other signatures (fig. S10C). These pairs of gene signatures (Q2 versus Q4, Ly108+CD69+ versus Ly108-CD69+, and CD101-Tim3+ versus CD101+Tim3+) were not negatively correlated with their counterparts (fig. S10C). Therefore, we gated on cells on the basis of the ratio of Q2/Q4 signature scores within three distinct subsets—Gzmk+ early Tem, ZNF683+  $T_{RM}$ , and terminal  $T_{EX}$ —to test whether the Q2 and Q4 states represented divergent functional states within and across these subsets. Overall, the Q2/Q4 ratio HIGH cells showed higher expression of effector cytokine transcripts IFNG and TNF and lower exhaustion as compared with the Q2/Q4 ratio Cells within these subsets, although the extent of these differences varied (Fig. 7, D to F). In contrast, cells gated on the value of Ly108+CD69+/Ly108-CD69+ signature ratio were more

often indifferent or skewed in the opposite direction with respect to the same metrics (fig. S10A). The CD101<sup>-</sup>Tim3<sup>+</sup>/CD101<sup>+</sup>Tim3<sup>+</sup> ratio, although more variable, showed some similarities with the trends in the Q2/Q4 ratio (fig. S10B).

To use these gene signatures to query patient outcome data, we stratified patients with HNSC from The Cancer Genome Atlas (TCGA) using the same Q2 and Q4 signatures generated from HNSC CITE-Seq into the top and bottom 30% on the basis of the expression of the ratio of Q2/Q4 signature scores. Patients with HNSC and with gene expression patterns skewed toward the Q2 signature showed significantly better overall survival compared with those enriched for the Q4 signature (Fig. 7J). Patients scoring high on the Q2/Q4 ratio score showed significantly better overall survival in all indications combined (Fig. 7G). In contrast, the Ly108<sup>+</sup>CD69<sup>+</sup>/Ly108<sup>-</sup>CD69<sup>+</sup> signature ratio was indifferent to (Fig. 7H) and the CD101<sup>-</sup>Tim3<sup>+</sup>/CD101<sup>+</sup>Tim3<sup>+</sup>

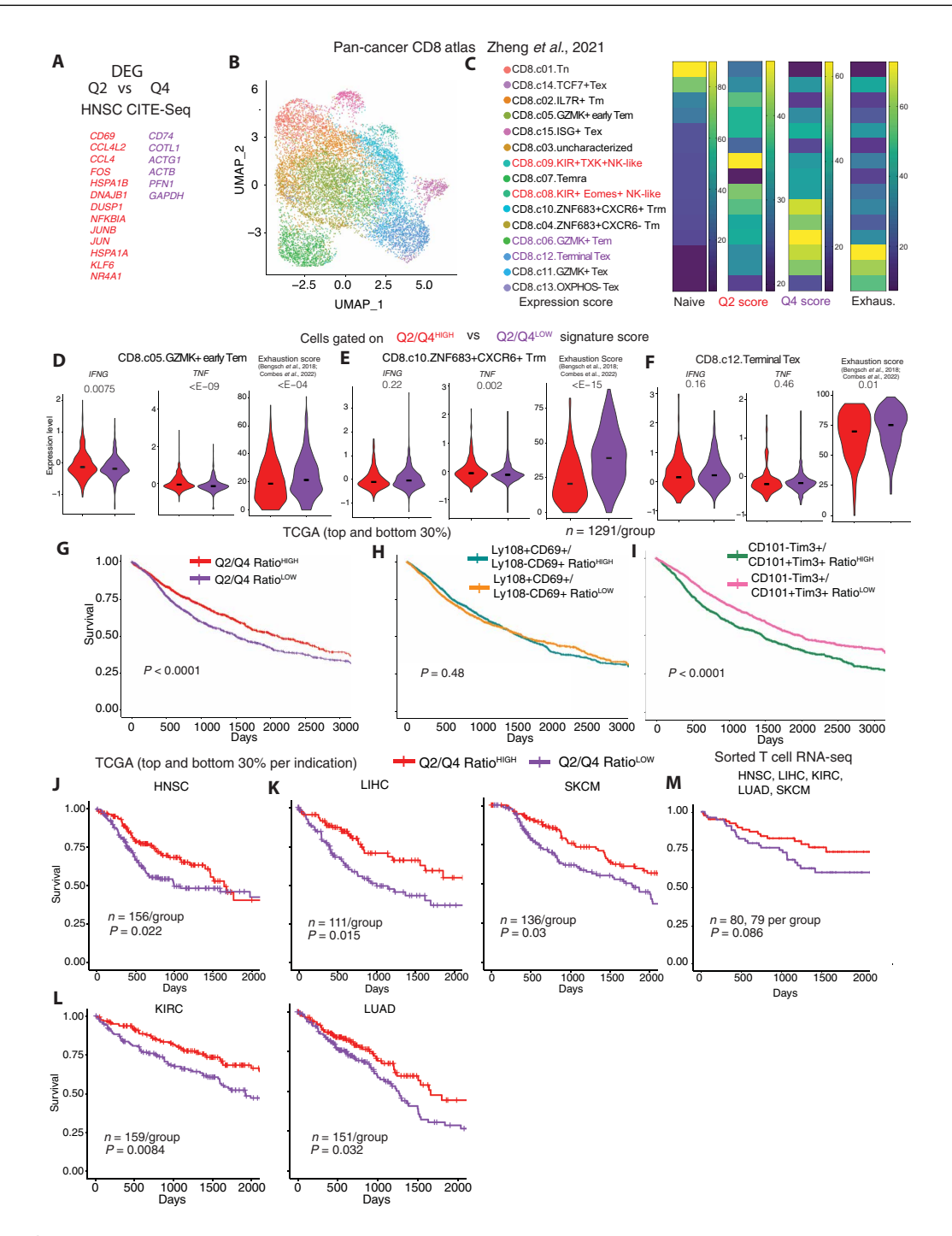


Fig. 7. A *CD69*<sup>hi</sup> (**Q2**) transcriptomic signature is associated with antitumor effector function across human cancers. (**A**) Differentially expressed genes of cells in Q2 versus Q4 ([avg\_logFC] > 0.4, pval\_adj < 0.01) from the HNSC CITE-Seq data in Fig. 6 used to generate Q2 and Q4 signature scores. (**B**) UMAP representation of computationally derived subsets among CD8 T cells in a pan-cancer T cell atlas (61); color-coded subset labels are as shown in (C). (**C**) Heatmap showing naïve (*SELL*, *IL7R*, *TCF7*, *LEF1*, and *CCR7*), Q2 [from (A)], Q4 [from (A)], and exhaustion (62) signature scores in the major CD8 T cell subsets from the same pan-cancer dataset. The top two subsets in Q2 and Q4 score expression are labeled red and purple, respectively, and clusters are arranged in descending order of expression of the naïve score. Expression of *IFNG*, *TNF*, and exhaustion signature score within the (**D**) early Tem, (**E**) CXCR6<sup>+</sup> T<sub>RM</sub>, and (**F**) terminal T<sub>EX</sub> clusters grouped by Q2/Q4<sup>high</sup> and Q2/Q4<sup>low</sup> (top and bottom 33% of the Q2 score/Q4 score ratio). (**G** to **I**) Kaplan-Meier survival curves from a quality-controlled subset of TCGA data (62) corresponding to all indications stratified by the ratio of (G) Q2 and Q4 expression scores, (H) signatures corresponding to Ly108<sup>+</sup>CD69<sup>+</sup> and Ly108<sup>-</sup>CD69<sup>+</sup> subsets [signature 1 and signature 7 from (11)], and (I) CD101<sup>-</sup>Tim3<sup>+</sup> effector and CD101<sup>+</sup>Tim3<sup>+</sup> terminal subsets (13). Kaplan-Meier survival curves from a curated list of TCGA data (62) corresponding to (J) HNSC, (**K**) LIHC and SKCM, and (L) KIRC and LUAD indications, with patients stratified by the ratio of Q2 and Q4 expression scores from bulk RNA-seq of sorted T cells (62). The number of patients per group and *P* value for log-rank tests are noted in (G) to (M), and *P* values for the Wilcoxon test in (D) to (F) are noted. Black bars represent medians in (D) to (F).

ratio correlated negatively (Fig. 7I) with patient survival in the same TCGA cohort. Although these results do not diminish the value of these previously described subsets for mapping T cell exhaustion, they support the *CD69* RNA—based delineation as a distinct additional categorization of biological and clinical relevance.

In addition to HNSC, Q2/Q4 ratio was a significant survival prognostic in multiple indications including hepatocellular (LIHC), melanoma (SKCM), didney (KIRC), and lung (LUAD) cancers (Fig. 7, K and L). Other indications [bladder (BLCA), colorectal (COAD), glioblastoma (GBM), gynecological (GYN), pancreatic (PAAD), and sarcoma (SRC)] remained neutral to overall survival (fig. S10, D and E). To test that this association with survival was T cell dependent, we used a smaller bulk RNA sequencing (RNA-seq) dataset from sorted intratumoral conventional T cells (62). Combining the abovementioned indications (LIHC, SKCM, KIRC, LUAD, and HNSC) where Q2/Q4 was associated with increased survival in TCGA, we found a distinct trend toward a similar association even in this smaller dataset (~80 patients per group) (Fig. 7M). Also consistent with the TCGA analysis, in this pan-cancer cohort, the T cell-specific Q2/Q4 ratio remained neutral to overall survival in other indications (BLCA, COAD, GBM, GYN, PAAD, and SRC) combined (fig. S10F). Although these distinct outcome cohorts may be attributed to the heterogeneity across cancer types, it is notable that, in none of the indications, this ratio emerges as a negative prognostic. Together, these data show that this delineation of CD69<sup>+</sup> CD8 T cells by CD69 RNA into potent and dysfunctional activation states is relevant in many human cancers. Delineating this axis of potent effector states by tracking CD69 RNA provides an additional dimension to map the contours of the exhaustion-dominated T cell functional landscape in tumors.

#### **DISCUSSION**

In summary, we have defined a multimodal approach using transcript and protein levels of CD69 simultaneously to identify potent effector CD8 T cell states that extend beyond the exhausted T cell lineage in tumors (fig. S11). Our data suggest that such states may be naturally prominent in certain TMEs (MC38) and rare in others (B78/B16), with functional consequences. By determining functional states associated with patterns of Cd69 RNA and protein expression, our data lend further relevance and context to the discordance between this transcript and its protein expression in T cells (41, 42). Associated with tissue retention (45, 55) or stimulation in general, the relationship between CD69 protein expression and intratumoral T cell function is ambiguous. In contrast, we show that higher expression of Cd69 RNA indicates a poised or potent activation state and therefore indicative of greater functional potential. The systematic use of Cd69 transcription, along with its surface protein expression, may be similarly applicable in other contexts, including vaccination, resident memory formation, and autoimmunity. Although the fast maturation time of monomeric TFP allows concordant recording of new transcription, the longer half-life of the fluorescent protein makes it insensitive to rapid changes as a reporter. Rather, the decline in TFP expression should be thought of as a delayed reporting of decreasing transcription integrated over a period of days. Furthermore, transcription and detectable mRNA may also be different under some conditions where mRNA degradation (42) dominates the posttranscriptional regulation. In this context, further studies using the inducible Cre in the reporter construct to

lineage-trace, image, or deplete activated cell states marked by the reporter may be leveraged to further understand the nuance of this biology.

Our results demonstrate that, among CD69<sup>+</sup> activated CD8 T cells, those with higher *Cd69* transcription, and associated higher levels of AP-1 TF expression, are functionally distinct from those with lower levels of these transcripts. These data are consistent with separate previous reports showing the overexpression of AP-1 factors JUN, STAT5A, and BATF in CD8 T cells leading to enhanced functional capacities (36–38). In the presence of AP-1 factors and NFAT, BATF can promote potent effector function and counteract exhaustion (38); our data indicate that this strategy of indirect recording of AP-1, NFAT activity by *Cd69* transcription illuminates those cells in which such functional signaling is active.

Accumulating evidence suggests that exhausted CD8 T cells in the TME continue to receive suboptimal TCR stimulation, keeping them locked in a dysfunctional activation state (20, 63). Within and across  $T_{EX}$  subsets, our data support the delineation of Q2 (Cd69RNAhi CD69protein+) and Q4 (Cd69RNAlo CD69protein+) as "potent" and "chronic" activation states, respectively. Conversely, Q1 (Cd69RNA<sup>hi</sup> CD69protein<sup>-</sup>) represents a "poised" state, whereas Q3 (Cd69RNAlo CD69protein) is a quiescent state encompassing both certain naïve and bystander cells, as well as inactive exhausted cells. In this way, these results are not meant to replace but add to the already existing mapping of T<sub>EX</sub> cell states. The application of this methodology in the CITE-Seq context demonstrates the potential to find functionally relevant activation states in human cancers. As such, the gene signatures for the divergent activation states derived from head and neck tumors may be further refined to be robust across species and indications, perhaps with the aid of bulk RNAseq or ATAC-seq (assay for transposase-accessible chromatin using sequencing) modalities.

The use of CD69 protein as a primary marker of specific T cell states is a point of consideration for future studies. Our data show that repetitive TCR stimulation and exposure to antigen-bearing TME are sufficient for the drop in relative transcription levels and TFP and the resultant functional differences between TFP<sup>hi</sup> and TFP<sup>lo</sup> subsets. However, given other stimuli that can induce CD69 expression, it is not necessary that Q2 and Q4 cells be produced by TCR-dependent mechanisms. It remains to be explored whether other forms of repetitive stimulation can drive such a feedback response associated with decreasing function. Overall, the interpretation of CD69 protein expression as it pertains to function likely depends on these additional measures of feedback.

Successful boosting of antitumor immunity in rare pockets of reactive immunity (1, 64, 65) may lead to the generation of stronger effector CD8 T cells, perhaps without entirely reversing the differentiation favoring exhaustion. Atypical effector states have been amplified by the specific deletion or overexpression of exhaustion lineage-defining TFs (17, 19). These and other data (35) suggest that the  $T_{\rm EX}$  cell subsets are not entirely devoid of plasticity. Although the overarching trajectory of CD8 T cell differentiation in tumors may be set by exhaustion lineage—defining factors, there appear to be local and global peaks and valleys of function that may be determined by additional axes of potency.

As exploration of spatial niches of functional immunity continue to drive the field, we posit that this approach toward directly marking the potent effectors in the TME may be an important anchoring tool. Detecting, studying, and ultimately enhancing functional antitumor CD8 T cells will lead to the discovery of novel strategies to drive better patient outcomes.

#### **MATERIALS AND METHODS**

#### Study design

The first part of this study was aimed at testing the utility of the Cd69-TFP mouse model reporting of the hysteresis of Cd69 transcription during T cell activation in vitro. Sample sizes of n = 3 or 4 biological replicates were used for most of these experiments. For mapping the same onto antigen-specific T cells in tumors, we used adoptive transfer in vivo and ex vivo tumor slices, with sample sizes in the range of n = 5 or 6 biological replicates owing to greater expected variability. For testing these in human CITE-Seq, we set a minimum threshold for n = 5 for the cohort and the final sample size (n = 7) was determined by resource and patient sample availability. Preexisting datasets were used without significant attrition; only the TCGA dataset was curated as described before to include only primary tumor samples. In most experiments, mice were randomized by cage, the experimenter was not fully blinded to treatment groups, and each experiment reported was repeated at least twice with the requisite biological replicates, except those generating sequencing data, which were only performed once. Outliers were not explicitly removed. End points in tumor studies, especially tumor growth studies, were determined by animal use protocol guidelines.

#### Mice

All mice were treated in accordance with the regulatory standards of the National Institutes of Health and American Association of Laboratory Animal Care and were approved by the UCSF Institution of Animal Care and Use Committee. Cd69-TFP-CreER<sup>T2</sup> (denoted as Cd69-TFP) mice in the C57BL/6J background were custom generated from Biocytogen Inc. and then maintained heterozygous (bred to C57BL/6J WT mice) at the UCSF Animal Barrier facility under specific pathogen-free conditions. C57BL/6J (WT), C57BL/6J CD45.1 (B6.SJL-Ptprc<sup>a</sup> Pepc<sup>b</sup>/BoyJ), and OT-I [C57BL/6-Tg (TcraTcrb)1100Mjb/J] mice were purchased for use from the Jackson Laboratory and maintained in the same facility in the C57BL/6J background. For adoptive transfer experiments, CD45.1 het; OT-Ihet; Cd69-TFPhet (denoted simply as CD45.1; OT-I; Cd69-TFP) mice were used. Mice of either sex ranging in age from 6 to 14 weeks were used for experimentation. For experiments using the transgenic PyMTchOVA strain (53), mammary tumor-bearing females in the age range of 15 to 24 weeks were used. Adoptive transfer of T cells in these mice was done when mice developed at least two palpable tumors (>25 to 30 mm<sup>2</sup>).

#### Mouse tumor processing and flow cytometry

The processing of tumors from mice to generate single-cell suspensions followed previously described protocols (66). Briefly, tumors were harvested and mechanically disintegrated on ice using razor blades, after which enzymatic digestion with DNAse (200 µg/ml Sigma-Aldrich), collagenase I (100 U/ml; Worthington Biochemical), and collagenase IV (500 U/ml; Worthington Biochemical) was performed for 30 min at 37°C while shaking. At the end of the digestion, the enzymes were quenched by adding excess 1× phosphate-buffered saline (PBS), filtered through a 100-µm mesh, and centrifuged, and red blood cells (RBCs) were removed by resuspending in RBC lysis

buffer (155 mM NH<sub>4</sub>Cl, 12 mM NaHCO<sub>3</sub>, and 0.1 mM EDTA) and incubating at room temperature for 10 min. The lysis buffer was quenched with excess  $1\times$  PBS, centrifuged, and resuspended in fluorescence-activated cell sorting (FACS) buffer [2 mM EDTA + 1% fetal calf serum (FCS) in  $1\times$  PBS] to obtain single-cell suspensions. Similarly, tumor-dLNs were isolated and digested with the same enzyme cocktail mashed directly over 100- $\mu$ m filters in PBS to generate single-cell suspensions.

For each tumor and lymph node sample, up to 2.5 million to 3 million cells per sample were stained in a total of 50 µl of antibody mixture for flow cytometry. Cells were centrifuged and washed with PBS prior to staining with Zombie NIR Fixable live/dead dye (1:500) (BioLegend) for 20 min at 4°C. Next, the samples were washed in FACS buffer followed by surface staining for 30 min at 4°C by resuspending in a mixture of directly conjugated antibodies (table S1) diluted in FACS buffer containing 1:100 anti-CD16/32 (Fc block; BioXCell) to block nonspecific binding. Antibody dilutions ranged from 1:100 to 1:400. After surface staining, cells were washed again with FACS buffer. For intracellular staining, cells were fixed for 20 min at 4°C either by using the IC Fixation Buffer (eBioscience) for cytoplasmic proteins or the TF fixation buffer (eBioscience) and washed in permeabilization buffer from the Foxp3/Transcription Factor Staining Buffer Set (eBioscience). Antibodies against intracellular targets were diluted in permeabilization buffer containing 1:100 Fc block, and cells were incubated for 30 min at 4°C followed by another wash prior to readout on a BD LSRII or Fortessa cytometer.

## Processing and flow cytometry analysis of other mouse organs

To phenotype T cells from lymphoid organs under homeostasis, the spleen and inguinal, mesenteric, and brachial lymph nodes were isolated and mashed over 100- $\mu$ m filters and washed with  $1\times$  PBS to generate single-cell suspension of lymphocytes. For splenic suspensions, RBC lysis was performed as described above before staining for flow cytometry.

To profile thymocytes, the thymus was isolated, cut into small pieces with a razor blade, and minced by using a gentleMACS dissociator (Miltenyi Biotec) in RPMI. Next, the mixture was spun down and resuspended in the digestion mixture described above and allowed to digest with shaking at 37°C for 20 min, after which the remaining tissue was either minced again using the gentleMACS dissociator and/or directly mashed over a 100-µm filter in FACS buffer to generate a single-cell suspension ready to be processed for staining and flow cytometry.

Skin digestion was done as previously described (*67*). Briefly, mice underwent shaving and hair removal prior to excision of the dorsal skin. Fat was peeled off the skin and cut into small pieces with scissors and razor blade in the presence of 1 ml of digest medium [collagenase IV (2 mg/ml; Roche), hyaluronidase (1 mg/ml; Worthington), and DNase I (0.1 mg/ml; Roche) in RPMI 1640 (Gibco)], until a paste-like consistency was achieved. The sample was then incubated at 37°C for 45 min with shaking and intermittent vortexing with 5 ml of additional digest solution. After being washed, the digested skin was passed through a 70- $\mu$ m strainer prior to staining. TFP high versus low gates were drawn by using a side-by-side WT control or using endogenous CD8 T cells in the context of adoptive transfer into a tumor-bearing mouse.

## Tumor injections and adoptive transfer of CD8 T cells into tumors

The B78chOVA and MC38chOVA cancer cell lines were generated by incorporating the same mCherry-OVA construct used to establish the PyMTchOVA spontaneous mouse line in our previous work (53) and have been used as previously described (22, 66). For tumor injections, the corresponding cells were grown to be >80% confluent in Dulbecco's modified Eagle's medium (DMEM) with 10% FCS (Benchmark) and 1% PSG (penicillin-streptomycin-glutamine, Gibco) and harvested using 0.05% or 0.25% trypsin-EDTA (Gibco). Cells were washed three times with PBS (Gibco) to prepare for the tumor injections. The requisite number of cells per injection was resuspended in PBS and mixed in a 1:1 ratio with Growth Factor Reduced Matrigel (Corning) to a final volume of 50 µl. The ice-cold mixture was injected subcutaneously into the flanks of anesthetized and shaved mice using a cold 29.5-gauge insulin syringe (BD Biosciences). CD8 T cells were isolated from CD45.1; OT-I; Cd69-TFP mice using the EasySep Negative Selection Kit (Stem Cell Bio) and resuspended in 1× PBS at 10× concentration, and 100 μl was injected into each tumor-bearing mouse. One million for B78chOVA and PyMTchOVA tumors and, for MC38chOVA tumors, 200,000 CD8 T cells were injected retro-orbitally into each mouse either 5 days (B78chOVA and MC38chOVA) after tumor injection or when mice had at least two palpable tumors (PyMTchOVA). Tumor measurements were done by measuring the longest dimension (length) and approximately perpendicular dimension (width) using digital calipers, rounded to one decimal place each.

#### Contralateral tumor injection and vaccination

Five days after B78chOVA tumor injection, equal numbers (1 million) of CD8 T cells from CD45.1; OT-I; Cd69-TFP and P14; Cd69-TFP mice were injected retro-orbitally into each mouse. Next day, gp33-41 subcutaneous peptide (Anaspec) vaccination was injected contralaterally to the tumor, with 50  $\mu g$  of peptide + 50  $\mu l$  of Freund's complete adjuvant (Sigma-Aldrich) along with 50  $\mu l$  of PBS for a total volume of 100  $\mu l$ . The vaccination site was identified by a white, hardened subcutaneous mass and isolated and processed similarly to the tumor for flow cytometry.

#### In vitro stimulation of naïve CD8 T cells

CD8 T cells were isolated from Cd69-TFP or WT mice as described above and plated in a 96-well round-bottom plate (Corning) at 80,000 cells per well in T cell media [RPMI (Gibco) + 10% FCS (Benchmark) + penicillin/streptomycin + glutamine (Gibco)]. TCR stimulation was induced by adding anti-CD3/CD28 Dynabeads (Applied Biosystems) at the concentration of 2 µl per 80,000 cells (1:1 ratio of cells:beads), the plate was briefly spun down to bring cells and beads together before incubation at 37°C for varying lengths of time. β-Mercaptoethanol (BME; Gibco) (55 μM) was added to the T cell medium during stimulation. For repeated stimulation assays, two wells of each sample at every time point were pooled for mRNA isolation and quantitative reverse transcription polymerase chain reaction (qRT-PCR), whereas two other wells were used as duplicates for flow cytometry. After each cycle, beads were taken off each well and replated for resting in T cell medium containing IL-2 (10 U/ml; PeproTech). To restart each stimulation cycle, we pooled cells from each biological replicate and counted them, and Dynabeads were added at the appropriate concentration for a 1:1 ratio and

redistributed into wells for incubation. To assay shorter stimulation times (3, 6, and 18 hours), we carried out the same repeated stimulation and rest experiment but analyzed cells by flow cytometry at these early stimulation time points at each cycle.

For cytokine production assays, cells at the beginning of cycle 3 were sorted by TFPhi versus TFPlo levels, with the nonreporter expressing control cells used to set the gate. Sorted cells were plated in a 96-well V-bottom plate either in T cell medium or T cell medium containing PMA (50 ng/ml; Sigma-Aldrich), ionomycin (500 ng/ml; Invitrogen) + brefeldin A (3  $\mu$ g/ml; Sigma-Aldrich), and BME (Gibco) for 3 hours before cells were collected for surface and intracellular staining for cytokines and GzmB.

## Sorting and qPCR, resting, or restimulation of homeostatic CD8 T cells

To sort sufficient CD8 T cells from homeostatic lymphoid organs, CD8 T cells were first isolated from spleens and inguinal, brachial, and mesenteric lymph nodes of Cd69-TFP or WT mice using the EasySep Negative selection kit. These cells were then sorted on TFPhi (top 15%), TFP<sup>mid</sup> (middle 30%), and TFP<sup>lo</sup> (bottom 15%) from each mouse separately and rested in T cell medium containing IL-7 (10 U/ml) in a 96-well round-bottom plate and assayed at 0, 24, and 48 hours. Likewise, for qPCR analysis, populations high, mid, and low for TFP were sorted into cold T cell medium, pelleted, and subjected to RNA extraction and qPCR with primers for Cd69 and 18S rRNA as the reference gene. For the sort and restimulation experiment, memory (CD44+CD62L+) TFPhi cells and effector (CD44<sup>+</sup>CD62L<sup>-</sup>) TFP<sup>lo</sup> cells were sorted and incubated in T cell media + 55 μM BME containing 1:1 anti CD3/CD28 Dynabeads in a 96-well round-bottom plate with either actinomycin D (5 μg/ml; Sigma-Aldrich) in dimethyl sulfoxide (DMSO) or DMSO alone (vehicle) for 3 hours before profiling by flow cytometry. De novo CD69 surface expression was measured by the difference of CD69 MFI between the vehicle and actinomycin D-treated groups.

## Restimulation and cytokine production of intratumoral CD8 T cells

OT-I T cells from B78chOVA tumors were sorted on a BD FACSAria Fusion or BD FACSAria2 (BD Biosciences) at d11 to d13 postadoptive transfer of CD8 T cells from CD45.1; OT-I; Cd69-TFP mice, as described above. To prepare CD45-enriched fractions (68), we digested tumors as described above into single-cell suspensions, centrifuged, and resuspended in 30 ml of room temperature RPMI 1640. Then, 10 ml of Ficoll-Premium 1.084 (Cytiva) was carefully underlaid, and the tubes were centrifuged at 1025g for 20 min at room temperature without braking. The resulting interface-localized cells were pipetted out, diluted in equal volume RPMI, and centrifuged at 650g for 5 min to collect the cells. This constituted a CD45-enriched fraction, which was then processed for staining and FACS. The four CD69:TFP quadrants were sorted from each tumor sample (cells from two or three tumor samples were pooled for a single biological replicate) into serum-coated microcentrifuge tubes containing cold T cell medium. These were subsequently plated in a 96-well V-bottom plate either in T cell medium or T cell medium containing PMA (50 ng/ml; Sigma-Aldrich), ionomycin (500 ng/ml; Invitrogen) + brefeldin A (3 µg/ml; Sigma-Aldrich), and BME (Gibco) for 3 hours before cells were collected for surface and intracellular staining for cytokines and GzmB.

To determine the conversion trajectory of CD69:TFP quadrants, intratumoral OT-I T cells were similarly sorted by CD69:TFP gating and restimulated with excess anti CD3/CD28 Dynabeads in a 96-well V-bottom plate for 3 days. Because of dearth of Q1 cells in the tumors at d12, we sorted those cells from the dLN instead. The resulting restimulated cells were assayed by flow cytometry to determine converted CD69:TFP quadrant distributions from each group.

#### Statistical analysis

Statistical analysis was done in GraphPad Prism or in R. For testing null hypothesis between two groups, either Student's t tests and or the nonparametric Mann-Whitney U tests were used, depending on the number and distribution of data points. Likewise, for testing null hypotheses among three or more groups, analysis of variance (ANOVA) or nonparametric tests were performed, followed by Tukey post hoc or Holm-Šidák's test, correcting for multiple comparisons. For multivariate datasets, two-way ANOVA was used with Tukey post hoc or post hoc Šidák's test for multiple comparisons. For testing CD69:TFP quadrant distributions over time, each quadrant was treated separately because these are not independent variables, with one-way ANOVA within each quadrant used for statistical testing. For both one-way and two-way ANOVA, when multiple comparisons were done across all possible pairwise comparisons, the Tukey's test was used, whereas the Holm-Šidák/Šidák's test was used for preselected pairwise comparisons. All data except RNA-seq are representative of at least two independent experiments.

#### **Supplementary Materials**

The PDF file includes:

Supplemental Materials and Methods Figs. S1 to S11 Table S1 References (70–76)

Other Supplementary Material for this manuscript includes the following:

Date file S1

 ${\sf MDAR\ Reproducibility\ Checklist}$ 

#### **REFERENCES AND NOTES**

- M. L. Broz, M. Binnewies, B. Boldajipour, A. E. Nelson, J. L. Pollack, D. J. Erle, A. Barczak, M. D. Rosenblum, A. Daud, D. L. Barber, S. Amigorena, L. J. van't Veer, A. I. Sperling, D. M. Wolf, M. F. Krummel, Dissecting the tumor myeloid compartment reveals rare activating antigen-presenting cells critical for T cell immunity. *Cancer Cell* 26, 938 (2014).
- H. Salmon, J. Idoyaga, A. Rahman, M. Leboeuf, R. Remark, S. Jordan, M. Casanova-Acebes, M. Khudoynazarova, J. Agudo, N. Tung, S. Chakarov, C. Rivera, B. Hogstad, M. Bosenberg, D. Hashimoto, S. Gnjatic, N. Bhardwaj, A. K. Palucka, B. D. Brown, J. Brody, F. Ginhoux, M. Merad, Expansion and activation of CD103<sup>+</sup> dendritic cell progenitors at the tumor site enhances tumor responses to therapeutic PD-L1 and BRAF inhibition. *Immunity* 44, 924–938 (2016).
- M. J. Pittet, M. Di Pilato, C. Garris, T. R. Mempel, Dendritic cells as shepherds of T cell immunity in cancer. *Immunity* 56, 2218–2230 (2023).
- B. Ruffell, D. Chang-Strachan, V. Chan, A. Rosenbusch, C. M. T. Ho, N. Pryer, D. Daniel, E. S. Hwang, H. S. Rugo, L. M. Coussens, Macrophage IL-10 blocks CD8<sup>+</sup>T cell-dependent responses to chemotherapy by suppressing IL-12 expression in intratumoral dendritic cells. *Cancer Cell* 26, 623–637 (2014).
- D. Masopust, S. J. Ha, V. Vezys, R. Ahmed, Stimulation history dictates memory CD8 T cell phenotype: Implications for prime-boost vaccination. *J. Immunol.* 177, 831–839 (2006).
- B. B. Au-Yeung, J. Zikherman, J. L. Mueller, J. F. Ashouri, M. Matloubian, D. A. Cheng, Y. Chen, K. M. Shokat, A. Weiss, A sharp T-cell antigen receptor signaling threshold for T-cell proliferation. *Proc. Natl. Acad. Sci. U.S.A.* 111, E3679–E3688 (2014).
- J. N. Mandl, J. P. Monteiro, N. Vrisekoop, R. N. Germain, T cell-positive selection uses self-ligand binding strength to optimize repertoire recognition of foreign antigens. *Immunity* 38, 263–274 (2013).

- A. Schietinger, M. Philip, V. E. Krisnawan, E. Y. Chiu, J. J. Delrow, R. S. Basom, P. Lauer, D. G. Brockstedt, S. E. Knoblaugh, G. J. Hämmerling, T. D. Schell, N. Garbi, P. D. Greenberg, Tumor-specific T cell dysfunction Is a dynamic antigen-driven differentiation program initiated early during tumorigenesis. *Immunity* 45, 389–401 (2016).
- A. C. Scott, F. Dündar, P. Zumbo, S. S. Chandran, C. A. Klebanoff, M. Shakiba, P. Trivedi, L. Menocal, H. Appleby, S. Camara, D. Zamarin, T. Walther, A. Snyder, M. R. Femia, E. A. Comen, H. Y. Wen, M. D. Hellmann, N. Anandasabapathy, Y. Liu, N. K. Altorki, P. Lauer, O. Levy, M. S. Glickman, J. Kaye, D. Betel, M. Philip, A. Schietinger, TOX is a critical regulator of tumour-specific T cell differentiation. *Nature* 571, 270–274 (2019).
- O. Khan, J. R. Giles, S. McDonald, S. Manne, S. F. Ngiow, K. P. Patel, M. T. Werner, A. C. Huang, K. A. Alexander, J. E. Wu, J. Attanasio, P. Yan, S. M. George, B. Bengsch, R. P. Staupe, G. Donahue, W. Xu, R. K. Amaravadi, X. Xu, G. C. Karakousis, T. C. Mitchell, L. M. Schuchter, J. Kaye, S. L. Berger, E. J. Wherry, TOX transcriptionally and epigenetically programs CD8<sup>+</sup>T cell exhaustion. *Nature* 571, 211–218 (2019).
- J. C. Beltra, S. Manne, M. S. Abdel-Hakeem, M. Kurachi, J. R. Giles, Z. Chen, V. Casella,
  S. F. Ngiow, O. Khan, Y. J. Huang, P. Yan, K. Nzingha, W. Xu, R. K. Amaravadi, X. Xu,
  G. C. Karakousis, T. C. Mitchell, L. M. Schuchter, A. C. Huang, E. J. Wherry, Developmental relationships of four exhausted CD8<sup>+</sup>T cell subsets reveals underlying transcriptional and epigenetic landscape control mechanisms. *Immunity* 52, 825–841.e8 (2020).
- B. Daniel, K. E. Yost, S. Hsiung, K. Sandor, Y. Xia, Y. Qi, K. J. Hiam-Galvez, M. Black, C. J. Raposo, Q. Shi, S. L. Meier, J. A. Belk, J. R. Giles, E. J. Wherry, H. Y. Chang, T. Egawa, A. T. Satpathy, Divergent clonal differentiation trajectories of T cell exhaustion. *Nat. Immunol.* 23, 1614–1627 (2022).
- W. H. Hudson, J. Gensheimer, M. Hashimoto, A. Wieland, R. M. Valanparambil, P. Li, J. X. Lin, B. T. Konieczny, S. J. Im, G. J. Freeman, W. J. Leonard, H. T. Kissick, R. Ahmed, Proliferating transitory T cells with an effector-like transcriptional signature emerge from PD-1<sup>+</sup> stem-like CD8<sup>+</sup>T cells during chronic infection. *Immunity* 51, 1043–1058.e4 (2019).
- E. J. Wherry, S. J. Ha, S. M. Kaech, W. N. Haining, S. Sarkar, V. Kalia, S. Subramaniam, J. N. Blattman, D. L. Barber, R. Ahmed, Molecular signature of CD8<sup>+</sup>T cell exhaustion during chronic viral infection. *Immunity* 27, 670–684 (2007).
- M. Philip, L. Fairchild, L. Sun, E. L. Horste, S. Camara, M. Shakiba, A. C. Scott, A. Viale, P. Lauer, T. Merghoub, M. D. Hellmann, J. D. Wolchok, C. S. Leslie, A. Schietinger, Chromatin states define tumour-specific T cell dysfunction and reprogramming. *Nature* 545, 452–456 (2017).
- D. T. Utzschneider, S. S. Gabriel, D. Chisanga, R. Gloury, P. M. Gubser, A. Vasanthakumar, W. Shi, A. Kallies, Early precursor T cells establish and propagate T cell exhaustion in chronic infection. *Nat. Immunol.* 21, 1256–1266 (2020).
- C. Tsui, L. Kretschmer, S. Rapelius, S. S. Gabriel, D. Chisanga, K. Knöpper, D. T. Utzschneider, S. Nüssing, Y. Liao, T. Mason, S. V. Torres, S. A. Wilcox, K. Kanev, S. Jarosch, J. Leube, S. L. Nutt, D. Zehn, I. A. Parish, W. Kastenmüller, W. Shi, V. R. Buchholz, A. Kallies, MYB orchestrates T cell exhaustion and response to checkpoint inhibition. *Nature* 609, 354–360 (2022).
- N. Prokhnevska, M. A. Cardenas, R. M. Valanparambil, E. Sobierajska, B. G. Barwick, C. Jansen, A. Reyes Moon, P. Gregorova, L. delBalzo, R. Greenwald, M. A. Bilen, M. Alemozaffar, S. Joshi, C. Cimmino, C. Larsen, V. Master, M. Sanda, H. Kissick, CD8<sup>+</sup> T cell activation in cancer comprises an initial activation phase in lymph nodes followed by effector differentiation within the tumor. *Immunity* 56, 107–124.e5 (2023).
- Z. Chen, Z. Ji, S. F. Ngiow, S. Manne, Z. Cai, A. C. Huang, J. Johnson, R. P. Staupe,
  B. Bengsch, C. Xu, S. Yu, M. Kurachi, R. S. Herati, L. A. Vella, A. E. Baxter, J. E. Wu, O. Khan,
  J. C. Beltra, J. R. Giles, E. Stelekati, L. M. McLane, C. W. Lau, X. Yang, S. L. Berger, G. Vahedi,
  H. Ji, E. J. Wherry, TCF-1-centered transcriptional network drives an effector versus
  exhausted CD8 T cell-fate decision. *Immunity* 51, 840–855.e5 (2019).
- H. Li, A. M. van der Leun, I. Yofe, Y. Lubling, D. Gelbard-Solodkin, A. C. J. van Akkooi, M. van den Braber, E. A. Rozeman, J. B. A. G. Haanen, C. U. Blank, H. M. Horlings, E. David, Y. Baran, A. Bercovich, A. Lifshitz, T. N. Schumacher, A. Tanay, I. Amit, Dysfunctional CD8 T cells form a proliferative, dynamically regulated compartment within human melanoma. *Cell* 176, 775–789.e18 (2019).
- H. E. Ghoneim, Y. Fan, A. Moustaki, H. A. Abdelsamed, P. Dash, P. Dogra, R. Carter, W. Awad, G. Neale, P. G. Thomas, B. Youngblood, De novo epigenetic programs inhibit PD-1 blockade-mediated T cell rejuvenation. *Cell* 170, 142–157.e19 (2017).
- K. Kersten, K. H. Hu, A. J. Combes, B. Samad, T. Harwin, A. Ray, A. A. Rao, E. Cai, K. Marchuk, J. Artichoker, T. Courau, Q. Shi, J. Belk, A. T. Satpathy, M. F. Krummel, Spatiotemporal co-dependency between macrophages and exhausted CD8<sup>+</sup> T cells in cancer. *Cancer Cell* 40, 624–638.e9 (2022).
- B. L. Horton, D. M. Morgan, N. Momin, M. Zagorulya, E. Torres-Mejia, V. Bhandarkar, K. D. Wittrup, J. C. Love, S. Spranger, Lack of CD8<sup>+</sup>T cell effector differentiation during priming mediates checkpoint blockade resistance in non–small cell lung cancer. *Sci. Immunol.* 6, eabi8800 (2021).
- A. C. Y. Chen, S. Jaiswal, D. Martinez, C. Yerinde, K. Ji, V. Miranda, M. E. Fung, S. A. Weiss, M. Zschummel, K. Taguchi, C. S. Garris, T. R. Mempel, N. Hacohen, D. R. Sen, The aged tumor microenvironment limits T cell control of cancer. *Nat. Immunol.* 25, 1033–1045 (2024).

- K. G. Anderson, I. M. Stromnes, P. D. Greenberg, Obstacles posed by the tumor microenvironment to T cell activity: A case for synergistic therapies. *Cancer Cell* 31, 311–325 (2017).
- J. M. Schenkel, K. A. Fraser, L. K. Beura, K. E. Pauken, V. Vezys, D. Masopust, Resident memory CD8 T cells trigger protective innate and adaptive immune responses. Science 346, 98–101 (2014).

SCIENCE IMMUNOLOGY | RESEARCH ARTICLE

- L. K. Mackay, M. Minnich, N. A. M. Kragten, Y. Liao, B. Nota, C. Seillet, A. Zaid, K. Man, S. Preston, D. Freestone, A. Braun, E. Wynne-Jones, F. M. Behr, R. Stark, D. G. Pellicci, D. I. Godfrey, G. T. Belz, M. Pellegrini, T. Gebhardt, M. Busslinger, W. Shi, F. R. Carbone, R. A. W. van Lier, A. Kallies, K. P. J. M. van Gisbergen, Hobit and Blimp1 instruct a universal transcriptional program of tissue residency in lymphocytes. Science 352, 459–463 (2016).
- F. A. Buquicchio, R. Fonseca, P. K. Yan, F. Wang, M. Evrard, A. Obers, J. C. Gutierrez,
  C. J. Raposo, J. A. Belk, B. Daniel, P. Zareie, K. E. Yost, Y. Qi, Y. Yin, K. F. Nico, F. M. Tierney,
  M. R. Howitt, C. A. Lareau, A. T. Satpathy, L. K. Mackay, Distinct epigenomic landscapes underlie tissue-specific memory T cell differentiation. *Immunity* 57, 2202–2215.e6 (2024).
- B. Virassamy, F. Caramia, P. Savas, S. Sant, J. Wang, S. N. Christo, A. Byrne, K. Clarke, E. Brown, Z. L. Teo, B. von Scheidt, D. Freestone, L. C. Gandolfo, K. Weber, J. Teply-Szymanski, R. Li, S. J. Luen, C. Denkert, S. Loibl, O. Lucas, C. Swanton, T. P. Speed, P. K. Darcy, P. J. Neeson, L. K. Mackay, S. Loi, Intratumoral CD8<sup>+</sup>T cells with a tissueresident memory phenotype mediate local immunity and immune checkpoint responses in breast cancer. Cancer Cell 41, 585–601.e8 (2023).
- F. Djenidi, J. Adam, A. Goubar, A. Durgeau, G. Meurice, V. de Montpréville, P. Validire, B. Besse, F. Mami-Chouaib, CD8<sup>+</sup>CD103<sup>+</sup> tumor-infiltrating lymphocytes are tumor-specific tissue-resident memory T cells and a prognostic factor for survival in lung cancer patients. *J. Immunol.* 194, 3475–3486 (2015).
- J. J. Milner, C. Toma, Z. He, N. S. Kurd, Q. P. Nguyen, B. M. Donald, L. Quezada, C. E. Widjaja,
  D. A. Witherden, J. T. Crowl, L. A. Shaw, G. W. Yeo, J. T. Chang, K. D. Omilusik, A. W. Goldrath,
  Heterogenous populations of tissue-resident CD8<sup>+</sup> T cells are generated in response to infection and malignancy. *Immunity* 52, 808–824.e7 (2020).
- M. Sade-Feldman, K. Yizhak, S. L. Bjorgaard, J. P. Ray, C. G. de Boer, R. W. Jenkins, D. J. Lieb, J. H. Chen, D. T. Frederick, M. Barzily-Rokni, S. S. Freeman, A. Reuben, P. J. Hoover, A. C. Villani, E. Ivanova, A. Portell, P. H. Lizotte, A. R. Aref, J. P. Eliane, M. R. Hammond, H. Vitzthum, S. M. Blackmon, B. Li, V. Gopalakrishnan, S. M. Reddy, Z. A. Cooper, C. P. Paweletz, D. A. Barbie, A. Stemmer-Rachamimov, K. T. Flaherty, J. A. Wargo, G. M. Boland, R. J. Sullivan, G. Getz, N. Hacohen, Defining T cell states associated with response to checkpoint immunotherapy in melanoma. Cell 175, 998–1013.e20 (2018).
- S. J. Im, M. Hashimoto, M. Y. Gerner, J. Lee, H. T. Kissick, M. C. Burger, Q. Shan, J. S. Hale, J. Lee, T. H. Nasti, A. H. Sharpe, G. J. Freeman, R. N. Germain, H. I. Nakaya, H. H. Xue, R. Ahmed, Defining CD8<sup>+</sup>T cells that provide the proliferative burst after PD-1 therapy. *Nature* 537, 417–421 (2016).
- M. L. Burger, A. M. Cruz, G. E. Crossland, G. Gaglia, C. C. Ritch, S. E. Blatt, A. Bhutkar,
  D. Canner, T. Kienka, S. Z. Tavana, A. L. Barandiaran, A. Garmilla, J. M. Schenkel, M. Hillman,
  I. de los Rios Kobara, A. Li, A. M. Jaeger, W. L. Hwang, P. M. K. Westcott, M. P. Manos,
  M. M. Holovatska, F. S. Hodi, A. Regev, S. Santagata, T. Jacks, Antigen dominance hierarchies shape TCF1<sup>+</sup> progenitor CD8 T cell phenotypes in tumors. *Cell* 184, 4996–5014.e26 (2021).
- S. E. McClory, O. Bardhan, K. S. Rome, J. R. Giles, A. E. Baxter, L. Xu, P. A. Gimotty, R. B. Faryabi, E. J. Wherry, W. S. Pear, M. S. Jordan, The pseudokinase Trib1 regulates the transition of exhausted T cells to a KLR<sup>+</sup> CD8<sup>+</sup> effector state, and its deletion improves checkpoint blockade. *Cell Rep.* 42, 112905 (2023).
- J. C. Beltra, M. S. Abdel-Hakeem, S. Manne, Z. Zhang, H. Huang, M. Kurachi, L. Su, L. Picton, S. F. Ngiow, Y. Muroyama, V. Casella, Y. J. Huang, J. R. Giles, D. Mathew, J. Belman, M. Klapholz, H. Decaluwe, A. C. Huang, S. L. Berger, K. C. Garcia, E. J. Wherry, Stat5 opposes the transcription factor Tox and rewires exhausted CD8<sup>+</sup>T cells toward durable effector-like states during chronic antigen exposure. *Immunity* 56, 2699–2718.e11 (2023).
- R. C. Lynn, E. W. Weber, E. Sotillo, D. Gennert, P. Xu, Z. Good, H. Anbunathan, J. Lattin, R. Jones, V. Tieu, S. Nagaraja, J. Granja, C. F. A. de Bourcy, R. Majzner, A. T. Satpathy, S. R. Quake, M. Monje, H. Y. Chang, C. L. Mackall, c-Jun overexpression in CART cells induces exhaustion resistance. *Nature* 576, 293–300 (2019).
- H. Seo, E. González-Avalos, W. Zhang, P. Ramchandani, C. Yang, C. J. Lio, A. Rao, P. G. Hogan, BATF and IRF4 cooperate to counter exhaustion in tumour-infiltrating CART cells. Nat. Immunol. 22, 983–995 (2021).
- J. F. Brooks, C. Tan, J. L. Mueller, K. Hibiya, R. Hiwa, V. Vykunta, J. Zikherman, Negative feedback by NUR77/Nr4a1 restrains B cell clonal dominance during early T-dependent immune responses. Cell Rep. 36, 109645 (2021).
- C. Tan, R. Hiwa, J. L. Mueller, V. Vykunta, K. Hibiya, M. Noviski, J. Huizar, J. F. Brooks, J. Garcia, C. Heyn, Z. Li, A. Marson, J. Zikherman, NR4A nuclear receptors restrain B cell responses to antigen when second signals are absent or limiting. *Nat. Immunol.* 21, 1267–1279 (2020).
- F. Salerno, M. Turner, M. C. Wolkers, Dynamic post-transcriptional events governing CD8<sup>+</sup> T cell homeostasis and effector function. *Trends Immunol.* 41, 240–254 (2020).

- associated with AU-rich sequence motifs. Eur. J. Immunol. 25, 2142–2146 (1995).
  F. Salerno, A. J. M. Howden, L. S. Matheson, Ö. Gizlenci, M. Screen, H. Lingel,
  M. C. Brunner-Weinzierl, M. Turner, An integrated proteome and transcriptome of B cell maturation defines poised activation states of transitional and mature B cells.
- Nat. Commun. 14, 5116 (2023).
  H. Weerakoon, A. Mohamed, Y. Wong, J. Chen, B. Senadheera, O. Haigh, T. S. Watkins, S. Kazakoff, P. Mukhopadhyay, J. Mulvenna, J. J. Miles, M. M. Hill, A. Lepletier, Integrative temporal multi-omics reveals uncoupling of transcriptome and proteome during human T cell activation. NPJ Syst. Biol. Appl. 10, 21 (2024).
- D. A. Walsh, H. Borges da Silva, L. K. Beura, C. Peng, S. E. Hamilton, D. Masopust,
  C. Jameson, The functional requirement for CD69 in establishment of resident memory
  CD8<sup>+</sup>T cells varies with tissue location. *J. Immunol.* 203, 946–955 (2019).
- C. Castellanos Mdel, S. Lopez-Giral, M. López-Cabrera, M. O. de Lándazuri, Multiple cis-acting elements regulate the expression of the early T cell activation antigen CD69. Eur. J. Immunol. 32, 3108–3117 (2002).
- J. F. Ashouri, A. Weiss, Endogenous Nur77 is a specific indicator of antigen receptor signaling in human T and B cells. J. Immunol. 198, 657–668 (2017).
- F. Salerno, S. Engels, M. van den Biggelaar, F. P. J. van Alphen, A. Guislain, W. Zhao,
  D. L. Hodge, S. E. Bell, J. P. Medema, M. von Lindern, M. Turner, H. A. Young, M. C. Wolkers,
  Translational repression of pre-formed cytokine-encoding mRNA prevents chronic activation of memory T cells. *Nat. Immunol.* 19, 828–837 (2018).
- A. J. Litterman, W. S. Zhu, R. Kageyama, W. Zhao, N. Zaitlen, D. J. Erle, K. M. Ansel, A global map of RNA binding protein occupancy guides functional dissection of posttranscriptional regulation of the T cell transcriptome. bioRxiv 448654 [Preprint] (2018). https://doi.org/10.1101/448654.
- M. J. Moore, N. E. Blachere, J. J. Fak, C. Y. Park, K. Sawicka, S. Parveen, I. Zucker-Scharff, B. Moltedo, A. Y. Rudensky, R. B. Darnell, ZFP36 RNA-binding proteins restrain T cell activation and anti-viral immunity. *eLife* 7, e33057 (2018).
- T. M. McCaughtry, M. S. Wilken, K. A. Hogquist, Thymic emigration revisited. *J. Exp. Med.* 204, 2513–2520 (2007).
- M. Yukawa, S. Jagannathan, S. Vallabh, A. V. Kartashov, X. Chen, M. T. Weirauch, A. Barski, AP-1 activity induced by co-stimulation is required for chromatin opening during T cell activation. J. Exp. Med. 217, e20182009 (2020).
- J. J. Engelhardt, B. Boldajipour, P. Beemiller, P. Pandurangi, C. Sorensen, Z. Werb, M. Egeblad, M. F. Krummel, Marginating dendritic cells of the tumor microenvironment cross-present tumor antigens and stably engage tumor-specific T cells. *Cancer Cell* 21, 402–417 (2012).
- N. E. Scharping, D. B. Rivadeneira, A. V. Menk, P. D. A. Vignali, B. R. Ford, N. L. Rittenhouse, R. Peralta, Y. Wang, Y. Wang, K. DePeaux, A. C. Poholek, G. M. Delgoffe, Mitochondrial stress induced by continuous stimulation under hypoxia rapidly drives T cell exhaustion. *Nat. Immunol.* 22, 205–215 (2021).
- J. G. Cyster, S. R. Schwab, Sphingosine-1-phosphate and lymphocyte egress from lymphoid organs. *Annu. Rev. Immunol.* 30, 69–94 (2012).
- R. You, J. Artichoker, A. Fries, A. W. Edwards, A. J. Combes, G. C. Reeder, B. Samad, M. F. Krummel, Active surveillance characterizes human intratumoral T cell exhaustion. J. Clin. Invest. 131, e144353 (2021).
- M. Y. Kasmani, R. Zander, H. K. Chung, Y. Chen, A. Khatun, M. Damo, P. Topchyan, K. E. Johnson, D. Levashova, R. Burns, U. M. Lorenz, V. L. Tarakanova, N. S. Joshi, S. M. Kaech, W. Cui, Clonal lineage tracing reveals mechanisms skewing CD8<sup>+</sup>T cell fate decisions in chronic infection. *J. Exp. Med.* 220, e20220679 (2023).
- B. C. Miller, D. R. Sen, R. al Abosy, K. Bi, Y. V. Virkud, M. LaFleur, K. B. Yates, A. Lako, K. Felt, G. S. Naik, M. Manos, E. Gjini, J. R. Kuchroo, J. J. Ishizuka, J. L. Collier, G. K. Griffin, S. Maleri, D. E. Comstock, S. A. Weiss, F. D. Brown, A. Panda, M. D. Zimmer, R. T. Manguso, F. S. Hodi, S. J. Rodig, A. H. Sharpe, W. N. Haining, Subsets of exhausted CD8<sup>+</sup>T cells differentially mediate tumor control and respond to checkpoint blockade. *Nat. Immunol.* 20, 326–336 (2019)
- J. J. Milner, C. Toma, B. Yu, K. Zhang, K. Omilusik, A. T. Phan, D. Wang, A. J. Getzler, T. Nguyen, S. Crotty, W. Wang, M. E. Pipkin, A. W. Goldrath, Runx3 programs CD8<sup>+</sup>T cell residency in non-lymphoid tissues and tumours. *Nature* 552, 253–257 (2017).
- B. Boldajipour, A. Nelson, M. F. Krummel, Tumor-infiltrating lymphocytes are dynamically desensitized to antigen but are maintained by homeostatic cytokine. *JCI Insight* 1, e89289 (2016).
- L. Zheng, S. Qin, W. Si, A. Wang, B. Xing, R. Gao, X. Ren, L. Wang, X. Wu, J. Zhang, N. Wu, N. Zhang, H. Zheng, H. Ouyang, K. Chen, Z. Bu, X. Hu, J. Ji, Z. Zhang, Pan-cancer single-cell landscape of tumor-infiltrating T cells. *Science* 374, abe6474 (2021).
- A. J. Combes, B. Samad, J. Tsui, N. W. Chew, P. Yan, G. C. Reeder, D. Kushnoor, A. Shen,
  B. Davidson, A. J. Barczak, M. Adkisson, A. Edwards, M. Naser, K. C. Barry, T. Courau,
  T. Hammoudi, R. J. Argüello, A. A. Rao, A. B. Olshen, C. Cai, J. Zhan, K. C. Davis, R. K. Kelley,
  J. S. Chapman, C. E. Atreya, A. Patel, A. I. Daud, P. Ha, A. A. Diaz, J. R. Kratz, E. A. Collisson,
  G. K. Fragiadakis, D. J. Erle, A. Boissonnas, S. Asthana, V. Chan, M. F. Krummel, M. Spitzer,

#### SCIENCE IMMUNOLOGY | RESEARCH ARTICLE

- L. Fong, A. Nelson, R. Kumar, J. Lee, A. Burra, J. Hsu, C. Hackett, K. Tolentino, J. Sjarif, P. Johnson, E. Shao, D. Abrau, L. Lupin, C. Shaw, Z. Collins, T. Lea, C. Corvera, E. Nakakura, J. Carnevale, M. Alvarado, K. Loo, L. Chen, M. Chow, J. Grandis, W. Ryan, I. el-Sayed, D. Jablons, G. Woodard, M. W. Meng, S. P. Porten, H. Okada, M. Tempero, A. Ko, K. Kirkwood, S. Vandenberg, D. Guevarra, E. Oropeza, C. Cyr, P. Glenn, J. Bolen, A. Morton, W. Eckalbar, Discovering dominant tumor immune archetypes in a pan-cancer census. *Cell* 185, 184–203.e19 (2022).
- C. U. Blank, W. N. Haining, W. Held, P. G. Hogan, A. Kallies, E. Lugli, R. C. Lynn, M. Philip, A. Rao, N. P. Restifo, A. Schietinger, T. N. Schumacher, P. L. Schwartzberg, A. H. Sharpe, D. E. Speiser, E. J. Wherry, B. A. Youngblood, D. Zehn, Defining 'T cell exhaustion'. Nat. Rev. Immunol. 19, 665–674 (2019).
- C. S. Jansen, N. Prokhnevska, V. A. Master, M. G. Sanda, J. W. Carlisle, M. A. Bilen, M. Cardenas, S. Wilkinson, R. Lake, A. G. Sowalsky, R. M. Valanparambil, W. H. Hudson, D. M. Guire, K. Melnick, A. I. Khan, K. Kim, Y. M. Chang, A. Kim, C. P. Filson, M. Alemozaffar, A. O. Osunkoya, P. Mullane, C. Ellis, R. Akondy, S. J. Im, A. O. Kamphorst, A. Reyes, Y. Liu, H. Kissick, An intra-tumoral niche maintains and differentiates stem-like CD8 T cells. Nature 576, 465-470 (2019).
- T. N. Schumacher, D. S. Thommen, Tertiary lymphoid structures in cancer. Science 375, eabf9419 (2022).
- K. C. Barry, J. Hsu, M. L. Broz, F. J. Cueto, M. Binnewies, A. J. Combes, A. E. Nelson, K. Loo, R. Kumar, M. D. Rosenblum, M. D. Alvarado, D. M. Wolf, D. Bogunovic, N. Bhardwaj, A. I. Daud, P. K. Ha, W. R. Ryan, J. L. Pollack, B. Samad, S. Asthana, V. Chan, M. F. Krummel, A natural killer-dendritic cell axis defines checkpoint therapy-responsive tumor microenvironments. *Nat. Med.* 24, 1178–1191 (2018).
- M. K. Ruhland, E. W. Roberts, E. Cai, A. M. Mujal, K. Marchuk, C. Beppler, D. Nam,
  N. K. Serwas, M. Binnewies, M. F. Krummel, Visualizing synaptic transfer of tumor antigens among dendritic cells. *Cancer Cell* 37, 786–799.e5 (2020).
- Y. S. Tan, Y. L. Lei, Isolation of tumor-infiltrating lymphocytes by Ficoll-Paque density gradient centrifugation. *Methods Mol. Biol.* 1960, 93–99 (2019).
- A. Ray, Mutlimodal\_Potent\_effector\_CD8\_Code, version v1, Zenodo (2025); https://doi. org/10.5281/zenodo.15444553.
- C. S. McGinnis, D. M. Patterson, J. Winkler, D. N. Conrad, M. Y. Hein, V. Srivastava, J. L. Hu, L. M. Murrow, J. S. Weissman, Z. Werb, E. D. Chow, Z. J. Gartner, MULTI-seq: Sample multiplexing for single-cell RNA sequencing using lipid-tagged indices. *Nat. Methods* 16, 619–626 (2019).
- E. Kim, R. Tyagi, J. Y. Lee, J. Park, Y. R. Kim, J. Beon, P. Y. Chen, J. Y. Cha, S. H. Snyder, S. Kim, Inositol polyphosphate multikinase is a coactivator for serum response factor-dependent induction of immediate early genes. *Proc. Natl. Acad. Sci. U.S.A.* 110, 19938–19943 (2013).
- A. S. Stephens, S. R. Stephens, N. A. Morrison, Internal control genes for quantitative RT-PCR expression analysis in mouse osteoblasts, osteoclasts and macrophages. BMC. Res. Notes 4, 410 (2011).

- A. Dobin, C. A. Davis, F. Schlesinger, J. Drenkow, C. Zaleski, S. Jha, P. Batut,
  M. Chaisson, T. R. Gingeras, STAR: Ultrafast universal RNA-seq aligner. *Bioinformatics* 29, 15–21 (2013).
- B. Li, C. N. Dewey, RSEM: Accurate transcript quantification from RNA-Seq data with or without a reference genome. BMC Bioinformatics 12, 323 (2011).
- H. G. Othmer, S. R. Dunbar, W. Alt, Models of dispersal in biological systems. J. Math. Biol. 26, 263–298 (1988).
- R. B. Dickinson, R. T. Tranquillo, Optimal estimation of cell movement indices from the statistical analysis of cell tracking data. AIChE J. 39, 1995–2010 (1993).

Acknowledgments: We thank E. Flynn (UCSF) for guidance with the CITE-Seq analysis. We thank J. Roose (UCSF), J. Zikherman (UCSF), and S. Schwab (NYU) for discussions and guidance. We thank K. Kersten, S.-B. Prebys, M. Kuhns (University of Arizona), and M. Reina-Campos (University of California San Diego) for critical reading of the manuscript. We also thank M. Reina-Campos for sharing data from Zheng et al. in an analysis-ready format. We thank members of the Krummel lab for inputs to the manuscript. Funding: This work was supported by the National Institutes of Health grants NIH R01CA197363 and NIH R37AI052116. A.R. was supported by a Cancer Research Institute Postdoctoral Fellowship (CRI2940). K.H.H. was supported by an American Cancer Society and Jean Perkins Foundation Postdoctoral Fellowship. G.H. was supported by the National Science Foundation Graduate Research Fellowship Program (NSF2034836). I.Z.-L. was supported by the Emerson Collective Health Research Scholars Program. Author contributions: Conceptualization: A.R. and M.F.K. Experimentation: A.R., M.B., G.H., L.F.P., and I.Z.-L. Mouse scSeq: K.H.H. and A.R. Human tumor data analysis: A.R., A.J.C., and B.S. Human tumor data collection: V.J., B.D., A.J.C., K.W., and P.H. Funding acquisition: M.F.K., A.R., and K.H.H. Writing: A.R. and M.F.K. Supervision: M.F.K. Competing Interests: The authors declare that they have no competing interests. Data and materials availability: New sequencing data are available at GEO as follows: human bulk RNA-seg, GEO accession GSE295725; human CITE-Seg, GEO accession GSE295704; and mouse scSeq data, GEO accession GSE295705. Computer codes used for analysis of sequencing data as well as cell migration data are available in the Zenodo repository (69). The Cd69-TFP mice are available for sharing from the corresponding author (matthew.krummel@ucsf.edu) and/or the first author (aray39@jh.edu), following execution of a material transfer agreement through the respective institutions. Data underlying the figures are provided in tabulated form in data file S1. All other data needed to evaluate the conclusions in the paper are present in the paper or the Supplementary Materials.

Submitted 23 September 2024 Resubmitted 7 February 2025 Accepted 21 May 2025 Published 11 July 2025 10.1126/sciimmunol.adt3537